United Aircraft Research Laboratories

UNITED AIRCRAFT CORPORATION

EAST HARTFORD, CONNECTICUT

D-910091-7

Experimental Investigation of Peripheral-Wall Injection Techniques in a Water Vortex Tube

NASA Contract No. NASw-847

REPORTED BY Arthur Travers
Arthur Travers

APPROVED BY William M. Foley
William M. Foley
Chief, Aerophysics Section

DATE September 1965

NO. OF PAGES 46

COPY NO. 23

FOREWORD

An exploratory experimental and theoretical investigation of gaseous nuclear rocket technology is being conducted by the United Aircraft Corporation Research Laboratories under Contract NASw-847 with the joint AEC-NASA Space Nuclear Propulsion Office. The Technical Supervisor of the Contract for NASA is Captain W. A. Yingling (USAF). Results of the investigation conducted during the period between September 15, 1964 and September 15, 1965 are described in the following eleven reports (including the present report) which comprise the required third Interim Summary Technical Report under the Contract:

1. McFarlin, D. J.: Experimental Investigation of the Effect of Peripheral Wall Injection Technique on Turbulence in an Air Vortex Tube. UAC Research Laboratories Report D-910091-5, September 1965. (Unclassified)

2. Johnson, B. V.: Analytical Study of Propellant Flow Requirements for Reducing Heat Transfer to the End Walls of Vortex-Stabilized Gaseous Nuclear Rocket Engines (U). UAC Research Laboratories Report D-910091-6, September 1965. (report classified Confidential)

3. Travers, A.: Experimental Investigation of Peripheral Wall Injection Techniques in a Water Vortex Tube. UAC Research Laboratories Report D-910091-7, September 1965. (Unclassified) (present report)

4. Johnson, B. V., and A. Travers: Analytical and Experimental Investigation of Flow Control in a Vortex Tube by End-Wall Suction and Injection (U). UAC Research Laboratories Report D-910091-8, September 1965. (report classified Confidential)

5. Mensing, A. E., and J. S. Kendall: Experimental Investigation of the Effect of Heavy-to-Light-Gas Density Ratio on Two-Component Vortex Tube Containment Characteristics (U). UAC Research Laboratories Report D-910091-9, September 1965. (report classified Confidential)

6. Krascella, N. L.: Theoretical Investigation of the Opacity of Heavy-Atom Gases. UAC Research Laboratories Report D-910092-4, September 1965. (Unclassified)

7. Kesten, A. S., and R. B. Kinney: Theoretical Effect of Changes in Constituent Opacities on Radiant Heat Transfer in a Vortex-Stabilized Gaseous Nuclear Rocket (U). UAC Research Laboratories Report D-910092-5, September 1965. (report classified Confidential)

8. Marteney, P. J., N. L. Krascella, and W. G. Burwell: Experimental Refractive Indices and Theoretical Small-Particle Spectral Properties of Selected Metals. UAC Research Laboratories Report D-910092-6, September 1965. (Unclassified)

9. Williamson, H. A., H. H. Michels, and S. B. Schneiderman: Theoretical Investigation of the Lowest Five Ionization Potentials of Uranium. UAC Research Laboratories Report D-910099-2, September 1965. (Unclassified)

10. McLafferty, G. H., H. H. Michels, T. S. Latham, and R. Roback: Analytical Study of Hydrogen Turbopump Cycles for Advanced Nuclear Rockets. UAC Research Laboratories Report D-910093-19, September 1965. (Unclassified)

11. McLafferty, G. H.: Analytical Study of the Performance Characteristics of Vortex-Stabilized Gaseous Nuclear Rocket Engines (U). UAC Research Laboratories Report D-910093-20, September 1965. (report classified Confidential)

Report D-910091-7

Experimental Investigation of Peripheral-Wall Injection Techniques in a Water Vortex Tube

TABLE OF CONTENTS

Report D-910091-7

Experimental Investigation of Peripheral-Wall Injection Techniques in a Water Vortex Tube

SUMMARY

An experimental investigation was conducted to determine the effects of the peripheral-wall injection technique used to drive a water vortex on the structure and thickness of the turbulent mixing region near the peripheral wall and on the flow patterns in the primary-flow region outside the peripheral and end-wall boundary layers. Three 10-in.-dia lucite vortex tubes having three different peripheral-wall injection configurations were tested: (1) tangential injection through a single 0.205-in.-high slot extending the entire 30-in. length of the tube, (2) tangential injection through four 0.050-in.-high slots, and (3) approximately tangential injection through 2144 ports of 0.060-in. diameter. In most tests, a controllable quantity of fluid was removed through one or more perforated screens in the peripheral wall, and the remainder of the fluid was removed through 0.938-in.-dia thru-flow ports located at the centers of the two end walls. However, a few tests were conducted in which no fluid was removed through the thru-flow ports; instead, fluid was injected through a 1.0-in.-dia porous tube located along the centerline of the vortex tube.

author

Microflash photographs of dye patterns were taken through one of the end walls to observe the characteristics of the turbulent mixing region, and time-exposure photographs of dye patterns were taken through the side wall to observe the characteristics of the primary-flow region. Tangential velocity profiles in the primary-flow region were obtained by means of a photographic particle-trace method using small, neutrally buoyant polystyrene spheres.

The results of the tests indicate that the volume of low-turbulence flow in the primary-flow region was considerably larger for the 2144-port injection configuration than for the single-slot and four-slot injection configurations. This larger volume is attributable to the much thinner turbulent mixing region near the peripheral wall for the 2144-port injection configuration.

RESULTS

1. Photographs of dye patterns indicated that the peripheral-wall turbulent mixing region was much thinner for the 2144-port injection configuration than for the single-slot and four-slot injection configurations. At thru-flow Reynolds numbers between 30 and 100, the resulting volume of low-turbulence flow in the primary-flow region of the vortex was 40% to 60% larger for the 2144-port injection configuration than for the other two injection configurations.

2. For a thru-flow Reynolds number equal to zero, the primary-flow region appeared less turbulent for the 2144-port injection configuration than for the other two injection configurations.

3. A radial stagnation surface (i.e., a surface of zero radial velocity) located near the outer boundary of the low-turbulence flow was observed for thru-flow Reynolds numbers up to 200 for the 2144-port injection configuration, but only up to thru-flow Reynolds numbers of 100 for the other two configurations.

4. An approximate analysis based on experimentally determined tangential velocity profiles indicated that for radial outflow conditions (obtained by injection of fluid through the centerline porous tube) the ratio of eddy viscosity to laminar viscosity increased with increasing injection rate.

INTRODUCTION

Gaseous nuclear rockets are potentially capable of providing values of specific impulse of 2000 to 3000 sec with thrust-to-weight ratios greater than unity. However, these performance capabilities will result in an economically attractive engine only if the nuclear fuel loss rates can be reduced substantially below the loss rates which would result from complete mixing of the fuel and propellant. Many different gaseous nuclear rocket concepts designed to minimize fuel loss rate have been proposed including some which are based on the suspension of gaseous nuclear fuel in a vortex. In all of these concepts, the fuel loss rates will be acceptably low only if the turbulence within the vortex is low.

The only known direct measurements of the turbulence within a vortex tube for different peripheral-wall injection techniques are reported in Ref. 1. In the configurations studied in Ref. 1, all of the flow injected into the vortex tube was removed through ports at the centers of the two end walls, which in effect fixed the ratio of the radial Reynolds number to the tangential injection Reynolds number. However, analytical studies conducted at the United Aircraft Research Laboratories (Ref. 2) have indicated that the flow pattern in a vortex, and hence possibly the turbulence level, is substantially modified at intermediate radii if this ratio is reduced. Such a reduction can be accomplished if the flow passing through the ports at the centers of the end walls is less than the total flow injected into the vortex tube (i.e., if a portion of the total flow injected is removed through the peripheral wall). It is also apparent (see Ref. 1) that the turbulence level in a vortex tube will be influenced by the peripheral-wall injection system used to inject fluid into the vortex. Such an injection system will influence turbulence both because of the high local injection velocities and because of the possible onset of Taylor-Goertler instabilities which occur in flows over concave walls (Ref. 3).

Two investigations were conducted to determine the effect of peripheral-wall injection configuration and the fraction of injected flow removed at the centerline of the end walls on vortex characteristics. The results of one of these investigations, which consisted of turbulence measurements in an air vortex, is described in Ref. 4. The second investigation, which was conducted in a water vortex using much of the same equipment used in Ref. 4, is described in the present report.

DESCRIPTION OF EQUIPMENT AND PROCEDURES

Description of Test Equipment

Vortex Tubes

Three transparent-wall water-vortex tubes having different peripheral-wall injection configurations were used. The geometry of a typical vortex tube is shown in Fig. 1 and details of the three injection configurations are shown in Fig. 2. In each case, the vortex was driven by injecting fluid nearly tangent to the peripheral wall through the respective injection configuration. A major portion of the flow, including most of the fluid which had lost angular momentum due to peripheral-wall skin friction, was removed through one or more perforated plates located in the wall (note peripheral bypass plenums in Fig. 2). The remainder of the injected fluid entered the primary-flow region and the end-wall boundary layers and was removed through thru-flow exhaust ports located at the center of each end wall (Fig. 1). Plain end walls which consisted of smooth lucite plates with thru-flow ports at the center were used in all tests.

A few tests were also conducted using the 2144-port injection configuration with additional fluid injection through a porous tube located along the centerline of the vortex tube. Data for these tests are discussed in the APPENDIX.

The single-slot injection configuration (Fig. 2) consisted of a 10-in.-dia lucite tube with a single 0.205-in.-high tangential injection slot extending the full 30-in. length of the tube. A peripheral bypass screen was located immediately upstream of the injection slot. A photograph of this configuration mounted on the test stand is shown in Fig. 3.

The four-slot injection configuration consisted of a 10-in.-dia inner structure with four injection plenums containing 0.050-in.-high tangential injection slots extending the full length of the tube. The injection slots were located 90-deg apart around the peripheral wall of the tube. The portions of the inner structure between the injection plenums were perforated and served as peripheral bypass screens. The inner structure was mounted concentrically in a 14-in.-dia lucite tube so that the annular volume between the inner structure and the outer tube served as a peripheral bypass plenum.

The 2144-port injection configuration consisted of a 10-in.-dia lucite tube with 2144 injection ports of 0.060-in. diameter. These ports were in 119 staggered circumferential rows (60 rows of 20 ports and 59 rows of 16 ports); the injection angle for all ports was 19 deg measured with respect to the tangent at the wall at the point of injection. A full-scale sketch of one quadrant of this injection configuration is shown in Fig. 4. Bypass screens and plenums extending the full

length of the vortex tube were located at 90-deg intervals around the peripheral wall. This 10-in.-dia tube was mounted concentrically in a 14-in.-dia lucite tube so that the annular volume between the two tubes served as an injection plenum. A photograph of this configuration is also shown in Fig. 3.

The injection area of the single-slot configuration was 6.15 sq in. The total injection areas of the four-slot and 2144-port configurations were approximately 6.00 sq in.

Flow Control System

Water was pumped from a storage tank through the injection plenums into the vortex tube. The desired flow conditions were obtained by separate adjustment of control valves downstream of the thru-flow ports and downstream of the peripheral bypass plenums. This method permitted independent control of the tangential injection and thru-flow Reynolds numbers.

Measurements of the total flow injected into the vortex tube were made using a turbine flowmeter located in the inlet flow pipe leading to the injection plenums. The thru-flow rate was determined in a similar manner by measuring the flow rate leaving the end-wall thru-flow ports. Measurements of water temperature were made using a thermometer located in the storage tank to determine the actual kinematic viscosity for calculating Reynolds numbers.

Optical System and Flow Visualization Techniques

Tangential velocities within the primary-flow region of the vortex were determined from time-exposure photographs of neutrally buoyant polystyrene spheres injected into the flow through the peripheral wall and end walls. A sketch of the optical system used to photograph the particles is shown in Fig. 5. The mercury vapor lamp was powered by a 1-kw, d-c power supply. The chopping disc contained 20 or 40 slots, depending on the flashing rate desired, and was driven by a variable-speed d-c shunt motor which allowed the flashing rate to be varied from 60 to 3000 flashes per sec. Intermittent illumination of the suspended particles caused them to appear as a series of streaks on a time exposure (see typical particle trace photograph in Fig. 6). This technique permitted quantitative evaluation of the tangential velocities within the confined vortex without using probes which would tend to disturb the flow.

To select test particles, small quantities of expandable polystyrene spheres were heated and then dispersed in water. Those which remained suspended after 30 minutes were drawn off, dried and sized. Particles selected in this manner were almost neutrally buoyant. The particles used in these tests ranged in diameter from 0.033 to 0.078 in.

Flow visualization was provided by injection of fluorescent dyes. Microflash photographs of dye patterns were taken through the end walls of the vortex tube with illumination through an adjustable slit (usually 1/4 in. wide) as shown in Fig. 5. The light source used for these photographs had a 0.1 microsecond flash period. Time exposure photographs of the dye patterns were also taken through the side wall of the vortex tube by interchanging the locations of the camera and light source as indicated in the note in Fig. 5 (the chopping wheel was not used). The exposure for these photographs was 1 sec at f/5.6.

Description of Test and Data Reduction Procedures

Range of Flow Conditions Investigated

The injection configurations and flow conditions which were investigated are summarized in the TABLE along with listings of the pertinent flow parameters. The average injection jet velocity was held constant at $V_j = 3.16$ ft/sec (corresponding to a constant injection jet volumetric flow rate of $Q_j = 0.135$ ft^3/sec) for all tests except those discussed in the APPENDIX. This jet velocity can be used to define a tangential injection Reynolds number using the following equation:

$$Re_{t,j} = \frac{\rho V_\phi r_1}{\mu} \tag{1}$$

For water at a temperature of 68 F, where the viscosity, μ, is 21.1×10^{-6} lb sec/ft^2, the tangential injection Reynolds number evaluated from Eq. (1) is 120,000.

Comparisons of the three different injection configurations in the following sections are made on the basis of the thru-flow radial Reynolds number, $Re_{r,t}$, as a parameter. This Reynolds number is defined as follows:

$$Re_{r,t} = \frac{\rho Q_t}{2\pi\mu L} \tag{2}$$

If all of the flow injected through the peripheral wall were removed from the ports at the centerline of the end walls, the resulting value of thru-flow Reynolds number at a water temperature of 68 F would be 780. All tests discussed in the main text of this report were conducted with values of $Re_{r,t}$ between 0 and 200. The tests discussed in the APPENDIX in which fluid was injected through a centerline porous tube were conducted with values of $Re_{r,t}$ between -3 and -100.

The TABLE also lists a parameter $\beta_{t,j}$. This parameter is related to the secondary-flow parameter β_t introduced in Ref. 2 where it was shown that confined

vortex flows having equal values of β_t would have similar flow patterns. As defined in Ref. 2,

$$\beta_t = \frac{(Re_{t_1})^{0.8}}{(Re_{r_1})} \cdot \frac{2r_1}{L} \tag{3}$$

where the radial and tangential Reynolds numbers are evaluated at the outer radius of the vortex tube. However, for the tests reported herein, the injection tangential Reynolds number, $Re_{t,j}$, was chosen as the most meaningful and reproducible parameter related to the tangential Reynolds number of Ref. 2. Similarly, since conditions in the interior of the flow field were difficult to set at specific values, the thru-flow Reynolds number, which is based on the thru flow withdrawn through the end walls rather than on the radial flow at r_1, was used instead. Thus, for these tests the secondary-flow similarity parameter was defined as

$$\beta_{t,j} = \frac{(Re_{t,j})^{0.8}}{Re_{r,t}} \cdot \frac{2r_1}{L} \tag{4}$$

When comparing data for different injection configurations for the same thru-flow rate, Q_t, the actual thru-flow and tangential Reynolds numbers usually differed substantially because of day-to-day variations in water temperature (see TABLE). However, note that for the same value of Q_t the values of $\beta_{t,j}$ based on actual water temperatures differed by at most 5%. This indicates that the variations in water temperature which occurred would not have significantly affected the flow patterns for the range of flow conditions tested. Accordingly, all of the data presented in this report (except where noted otherwise) are identified by nominal thru-flow and tangential Reynolds numbers based on the kinematic viscosity of water at 68 F. Equal values of these nominal Reynolds numbers correspond to equal thru-flow and injection volumetric flow rates for the different injection configurations.

Reduction of Particle-Trace Data

The first step in the procedure for obtaining local tangential velocities in the primary-flow region was to determine the radius of a particle-trace from a photograph (see Fig. 6). Two points at the ends of dashes were selected and the circumferential distance between them was calculated from the radius and the central angle subtended. The time of travel was determined from the number of dashes between the points and the light flashing rate. The tangential velocity was then calculated by dividing the circumferential distance by the time of travel.

A typical tangential velocity profile is shown in Fig. 7. Approximately 100 particle-trace data points were obtained for each profile. To obtain a profile, a fifth-order least-squares curve was fit through the data points using an IBM 7094

program. Brackets indicating one standard deviation of all points from the curve are shown in Fig. 7 to indicate typical scatter of the data.

DISCUSSION OF RESULTS

Characteristics of Turbulent Mixing Region Near Peripheral Wall

Microflash Photographs of Dye Patterns

Figures 8 through 13 contain microflash photographs of dye patterns taken through the end wall showing the effect of thru-flow Reynolds number on the turbulent structure of the flow near the peripheral wall for all three injection configurations. Although only one photograph is shown for each flow condition, many were taken. Those presented in this report were selected on the basis of clarity of the detail of the turbulent regions of the flow which were of primary interest in this investigation. In all photographs the flow rotation is counterclockwise (as indicated by the arrows) and the dye was injected through the peripheral wall at the axial midplane.

The dye pattern for the single-slot injection configuration in Fig. 8 for $Re_{r,t} = 0$ shows the existence of a large outer region of highly mixed flow characterized by diffuse dye streamers and a number of large eddies. The injection slot was located in the dark region at the left side of the photograph. A similar pattern is shown in the photograph for the four-slot injection configuration. In the photograph for the 2144-port injection configuration, the turbulent mixing region is shown to be confined to a smaller region between a radius of about $r = 4.0$ in. and the peripheral wall. However, at radii less than $r = 4.0$ in. the photograph shows stratified streamers of dye, indicating that a lower turbulence level existed in the primary-flow region than for the other two injection configurations. It should be noted that the axes of the eddies shown in Fig. 8 are along the length of the vortex tube. In the case of the Taylor-Goertler instabilities normally encountered in flow over concave surfaces (Ref. 3), the axes would be along the circumference of the tube, i.e., locally parallel to the wall. However, it was not possible to obtain clear photographs from the side of the tube in the region immediately adjacent to the peripheral wall. Such a view would be required to show Taylor-Goertler cells.

For a thru-flow Reynolds number of 30 (Fig. 9), the dye pattern near the peripheral wall of the single-slot injection configuration is characterized by a large number of wisps of dye shedding off the dense dye streamers caused by eddies which extend from a radius of approximately 3.5 in. to the peripheral wall (i.e., the mixing region thickness is approximately 1.5 in.). The complete eddies are not visible in the photographs due to the high turbulence near the wall which rapidly diffuses the dye. For the four-slot injection configuration, large eddies are also evident near the peripheral wall. The mixing region extends from a radius of approximately 3.0 in. to the peripheral wall. In contrast to the single-slot and four-slot injection configurations, the 2144-port injection configuration shows a fine stratified

flow out to a radius of approximately 4.5 in. In this case, the turbulent mixing region is confined to the portion of the vortex tube within approximately 1/2 in. of the wall.

The microflash photographs for a thru-flow Reynolds number of 60 show similar flow characteristics (Fig. 10). For the single-slot injection configuration, diffuse wisps of dye moving radially outward from the dense dye streamer can be seen. The turbulent mixing region extends from about a radius of approximately 3.5 in. to the peripheral wall as it did for this configuration at a thru-flow Reynolds number of 30. For the four-slot injection configuration a number of well-defined large eddies can be seen along the peripheral wall. Insufficient dye in the adjoining interior region prevented the full extent of the mixing region to be visible in this photograph; however, the photographs in Figs. 9 and 11 for the four-slot injection configuration show the radial extent of this region quite clearly. In Fig. 10, the photograph for the 2144-port injection configuration again shows a thin mixing region. However, outside this region (radially inward) a number of well-defined flattened eddies appear which do not extend to the peripheral wall. These eddies were observed at several thru-flow Reynolds numbers in regions away from the peripheral wall. They are not believed to be connected with peripheral wall turbulence and appear to be a result of small-amplitude, long-period radial oscillations of the flow which were visible in the dye patterns. The source of the disturbance causing these oscillations is not definitely known. The photographs in Fig. 11 for $Re_{r,t} = 93$ show the same trends observed in Figs. 8, 9 and 10. The thinnest turbulent mixing region again occurred in the vortex tube with the 2144-port injection configuration.

For thru-flow Reynolds numbers of 125 and 200, only the single-slot and 2144-port injection configurations are compared (Figs. 12 and 13). Flow patterns similar to those at lower thru-flow Reynolds numbers were observed. As in previous photographs, eddy size and mixing region width are larger for the single-slot configuration than for the 2144-port configuration. For the single-slot injection configuration, nearly periodic wisps of dye progressing outward toward the peripheral wall from an inner dye region can be seen; for the 2144-port injection configuration, a thin diffuse cloud of dye exists in the vicinity of the peripheral wall. In Fig. 13, the presence of eddies near the peripheral wall of the 2144-port configuration can be detected (note the periodic light and dark shading of the dye in this region). Within the central region of the flow (inside of the mixing region) in this vortex tube configuration, the dye patterns show well-defined stratified dye streamers, although in Fig. 12 a flat roll eddy can be seen at a radius of about 4.0 in.

Although no quantitative estimate of the level of turbulence in the flow region near the peripheral wall can be made from the microflash photographs, the photographs clearly indicate that the eddy size and width of the turbulent mixing region were smallest for the 2144-port injection configuration at all thru-flow Reynolds numbers. The fact that well-defined eddies existed which had a periodicity that changed with

flow condition and vortex tube geometry is particularly interesting. Boundary layer turbulence, which is random in nature, is one method of momentum exchange between the inner, high-velocity flow and the low-velocity flow near the peripheral wall. For flow along concave walls, the formation of Taylor-Goertler cells -- which also have a periodic structure -- can provide an important additional means of transporting momentum to the peripheral wall. An additional momentum transport mechanism appears to have been present in these tests in the form of an azimuthal wave which evidenced itself as a series of periodic eddies whose axes of rotation were perpendicular to the axes of the classical Taylor-Goertler cells. The cause of this instability is at present unknown.

Hot-Wire Anemometer Data

In the investigation reported in Ref. 4, hot-wire anemometer measurements were made to quantitatively determine the effect of the peripheral-wall injection technique on the level of turbulence in an air vortex. The vortex tubes and injection configurations tested were identical to the single-slot and 2144-port tubes used in the present investigation. Although air was used instead of water as the working fluid, data were obtained for approximately the same values of injection and thru-flow Reynolds numbers.

Figure 14 shows a comparison of turbulent energy spectra for the two configurations based on measurements made at a radius of 4.75 in. The flow conditions for these spectra correspond approximately to the flow conditions for the microflash photographs of dye patterns shown in Figs. 10 and 11 (actual $\beta_{t,j} \cong 56$). The measurements show large concentrations of energy at eddy wavelengths on the order of 1.0 in. for the single-slot injection configuration and 0.06 in. for the 2144-port injection configuration. Eddies having diameters on the order of 1.0 in. can be seen in the photographs in Figs. 9, 10 and 11 for the single-slot configuration, but the eddies at a radius of 4.75 in. in the 2144-port configuration are too small to be clearly distinguished.

Characteristics of Primary-Flow Region

Photographs of Dye Patterns

Figures 15 through 18 contain photographs of dye patterns taken through the side wall of the vortex tube showing the structure of the flow in the primary-flow region of the vortex for all three injection configurations. For these photographs, the dye was injected through ports in the end walls. The photographs were taken at the indicated times after cessation of dye injection.

Dye pattern photographs for a thru-flow Reynolds number of zero are shown in Fig. 15. For both the single-slot and four-slot configurations, the dye pattern is

very diffuse in the primary-flow region, which indicates a relatively high level of turbulence. Note in the photograph for the 2144-port injection configuration that ripples appear in the stratified dye streamers. This is due to a standing-wave instability in the primary-flow region which was observed for all three injection configurations at a thru-flow Reynolds number of zero. In an end view, the ripples appear as a series of ellipses with major axes alternately 90 deg apart along the axis of the vortex tube. However, in the 2144-port injection configuration, the presence of stratified dye filaments indicates a markedly less turbulent primary-flow region than for both the single-slot and four-slot injection configurations. The dye also appeared stratified in the microflash photograph taken through the end wall at this thru-flow Reynolds number (Fig. 8).

Figures 16, 17 and 18 show the structure of the flow for thru-flow Reynolds numbers of 30, 60 and 93, respectively. All photographs show axial recirculation cells in the primary-flow regions of the vortexes. The recirculation cells are enclosed by radial stagnation surfaces (surfaces of zero radial velocity). These surfaces coincide in radius near each end wall with the cell boundaries and are outlined by horizontal dye filaments in some of the photographs (e.g., see the lower photograph in Fig. 16). Outside of this surface the fluid moves axially toward the end walls. Inside of this surface, fluid leaves the end-wall boundary layer from a region near the center of the end wall, moves radially outward through the primary-flow region and then re-enters the end-wall boundary layer at radii slightly less than the radius of the radial stagnation surface. The flow inside of the radial stagnation surface appears to be laminar. Further descriptions of these recirculation cells are given in Ref. 2.

The location of the radial stagnation surface appears to correlate with the observed thickness of the turbulent peripheral-wall mixing region. Figure 19 shows the effect of thru-flow Reynolds number on the radius of the radial stagnation surface for all three configurations (the curves are based on photographs similar to those in Figs. 16, 17 and 18). No radial stagnation surface existed at thru-flow Reynolds numbers larger than the values indicated by an asterisk (i.e., the outer edge of the dye annulus moved radially inward with time and the turbulence in the primary-flow region increased). Note that this effect occurred at thru-flow Reynolds numbers greater than 200 for the 2144-port injection configuration and greater than 100 for the other two configurations. Figure 19 also shows that the radius of the radial stagnation surface was considerably larger for the 2144-port injection configuration, as would be expected because of its thinner mixing region. These results indicate that the use of distributed injection ports instead of single or multiple injection slots provides an appreciable increase (40% to 60%) in the volume of the central region of low-turbulence flow.

Tangential Velocity Profiles

Figures 20 and 21 show the effect of thru-flow Reynolds number on the tangential velocity profiles in the primary-flow region of the vortex for the single-slot and 2144-port injection configurations. Tangential velocity profiles were not obtained for the four-slot injection configuration since, as shown in Fig. 19, the radius of the radial stagnation surface (and hence the volume of low-turbulence flow in the primary-flow region) was less for this configuration than for the other two configurations. The profiles shown were obtained using the particle-trace method.

Consider first the tangential velocity profiles for thru-flow Reynolds numbers of 30, 60 and 90 (i.e., flow conditions for which recirculation cells occur for both injection configurations) shown in Figs. 20 and 21. In the outer region of flow, the velocities for the single-slot injection configuration are lower than for the 2144-port injection configuration. This difference undoubtedly is due at least in part to the different mixing region widths for the two injection configurations. In the inner region of flow (r = 1.0 to 3.0 in.), the velocity profiles are nearly the same. For a thru-flow Reynolds number of zero (Fig. 20), the tangential velocity profile for the 2144-port injection configuration shows a weaker vortex and steeper velocity gradient at radii greater than 3.0 in. than for the single-slot injection configuration.

REFERENCES

1. Kendall, J. M.: Experimental Study of a Compressible Viscous Vortex. Jet Propulsion Laboratory Technical Report No. 32-290, June 5, 1962.

2. Anderson, O.: Theoretical Solutions for the Secondary Flow on the End Wall of a Vortex Tube. United Aircraft Research Laboratories Report R-2494-1, November 1961.

3. Schlichting, H.: Boundary Layer Theory. McGraw-Hill Book Co., Inc., New York, 1960.

4. McFarlin, D. J.: Experimental Investigation of the Effect of Peripheral Wall Injection Technique on Turbulence in an Air Vortex Tube. United Aircraft Research Laboratories Report D-910091-5, September 1965.

5. Sziklas, E. A.: Analysis of Centrifugal Separation of Gases in a Rotating-Gaseous-Core-Nuclear Rocket. United Aircraft Research Laboratories Report R-1686-1, April 1960.

6. Hocking, L. M.: An Example of Boundary Layer Formation. AIAA Journal, Vol. 1, No. 5, pp. 1222-23, May 1963.

LIST OF SYMBOLS

A_j	Total area of injection slots or ports at peripheral wall of vortex tube, ft^2
L	Length of vortex tube, 2.50 ft
n_r	Exponent in circulation equation, $V_\phi r \propto r^{n_r}$
Q_j	Volumetric flow rate of injection jet which drives vortex, ft^3/sec
Q_t	Volumetric flow rate in thru-flow ducts, ft^3/sec
r	Local radius from centerline of vortex tube, ft (except where noted otherwise)
r_1	Outer radius of vortex tube, ft
Re_{r_1}	Radial Reynolds number at outer radius of vortex tube, $(V_{r_1} r_1)/\nu$, dimensionless
$Re_{r,p}$	Local radial Reynolds number in primary-flow region, $(V_r r)/\nu$, dimensionless
$Re_{r,t}$	Nominal thru-flow Reynolds number (radial Reynolds number for radial outflow) based on fluid properties at 68 F, $Q_t/2\pi\nu L$, dimensionless
Re_{t_1}	Tangential Reynolds number based on tangential velocity at outer radius of vortex tube, $V_\phi r_1/\nu$, dimensionless
$Re_{t,j}$	Tangential Reynolds number based on average injection velocity, $V_j r_1/\nu = Q_j r_1/(A_j\nu)$, dimensionless
v	Fluctuating component of tangential velocity, ft/sec
V_j	Average injection velocity, Q_j/A_j , ft/sec
V_r	Local radial velocity in primary flow, ft/sec
V_ϕ	Local tangential velocity in primary flow, ft/sec
z	Distance measured in a direction parallel to the axis of the vortex tube from the axial midplane, ft
$\beta_{t,j}$	Dimensionless secondary flow similarity parameter, $(Re_{t,j}^{0.8}/Re_{r,t})(2r_1/L)$

LIST OF SYMBOLS (Cont'd.)

ϵ	Eddy viscosity, ft^2/sec
ν	Kinematic viscosity, ft^2/sec
μ	Laminar viscosity, lb sec/ft^2
ρ	Density of water, $slug/ft^3$

APPENDIX

APPROXIMATE MEASUREMENTS OF THE RATIO OF EDDY VISCOSITY TO LAMINAR VISCOSITY IN A VORTEX WITH RADIAL OUTFLOW

Method of Analysis

An analysis in which theoretical and experimental results are compared to obtain an estimate of the ratio of eddy viscosity to laminar viscosity for flow in a vortex with radial outflow is described in this APPENDIX. Radial outflow data were obtained using the 2144-port injection configuration with additional fluid injected radially outward from a porous tube located along the centerline of the vortex tube (see sketch in Fig. 22).

The flow in the primary-flow region was observed from dye photographs to be turbulent for all radial outflow conditions. In the analysis, the flow was assumed to have constant viscosity and constant radial mass flow equal at all radii to the mass flow of fluid issuing from the porous tube. For this type of flow, a velocity distribution of the form $V_\phi \propto r^{n_\Gamma - 1}$ is a solution to the Navier-Stokes equations (Refs. 5 and 6). The eddy viscosity was assumed to be constant in the primary-flow region and the local radial Reynolds number, $Re_{r,p}$, was assumed to be equal to the outflow radial Reynolds number, $Re_{r,t}$ (based on the outflow through the porous tube).

The exponent n_Γ was determined graphically from log-log plots of the experimentally determined circulation distributions, where the circulation is defined as the product of V_ϕ and r. On a plot of $\log V_\phi r$ vs $\log r$, the exponent n_Γ is the slope of a straight line fit through the data points. The experimental and theoretical exponents were then compared by calculating the ratio of theoretical radial mass flow to the experimental radial mass flow as follows:

$$\frac{(Re_{r,p})_{LAMINAR}}{(Re_{r,p})_{EXPERIMENTAL}} = \frac{(2 - n_\Gamma)_{LAMINAR}}{(2 - n_\Gamma)_{EXPERIMENTAL}} = \frac{\dfrac{\rho V_r r}{\mu}}{\dfrac{\rho V_r r}{\rho \epsilon + \mu}} = \frac{\rho \epsilon + \mu}{\mu} \qquad (5)$$

Thus, the ratio of eddy viscosity to laminar viscosity was obtained in terms of the experimental and theoretical values of n_Γ:

$$\frac{(2 - n_\Gamma)_{LAMINAR}}{(2 - n_\Gamma)_{EXPERIMENTAL}} = \frac{\rho \epsilon + \mu}{\mu} \cong \frac{\rho \epsilon}{\mu} \qquad (6)$$

It should be pointed out that for the analysis to be valid the eddy viscosity in the primary-flow region of the vortex must be nearly constant.

Discussion of Results

Figures 22 through 24 present the data employed in determining the experimental values of the exponent n_r . The effect of outflow radial Reynolds number on the tangential velocity profiles is shown in Fig. 22, and the scatter in the data for a typical circulation profile is shown in Fig. 23. Circulation profiles on log-log coordinates for the four outflow radial Reynolds numbers tested are shown in Fig. 24. The experimental value of n_r was determined graphically from the slope of the circulation profile in the radial region between 2.5 and 4.0 in., where the profiles are approximately linear. Little deviation in the measured exponent value was possible because of the small scatter in the data (see Fig. 23).

Comparison of the theoretical and experimental variations of n_r with outflow radial Reynolds number are shown in Fig. 25. Note that the experimental variation is almost flat compared with the steep gradient with increased outflow radial Reynolds number for the theoretical variation (i.e., for laminar flow). This difference is an indication of the turbulence which exists in the actual vortex with radial outflow.

The effect of outflow radial Reynolds number on the ratio of eddy viscosity to laminar viscosity (based on theoretical and experimental values of n_r from Fig. 25) is shown in Fig. 26. The ratio increases with increasing outflow radial Reynolds number. Photographs of dye patterns at the four outflow radial Reynolds numbers for which tangential velocity profiles were obtained are shown in Fig. 27.

TABLE

SUMMARY OF CONFIGURATIONS AND FLOW CONDITIONS FOR COMPLETE TEST PROGRAM

All data in figures and text identified by nominal $Re_{r,t}$ and $Re_{t,j}$ except where noted otherwise

INJECTION CONFIGURATION (See Fig. 2)	FLOW CONDITIONS									FIGURES ON WHICH DATA ARE PRESENTED	
	Thru-Flow Rate, Q_t-gpm	Nominal Thru-Flow or Radial Reynolds Number at 68 F, $Re_{r,t}$	Water Temperature T-deg F	Actual Thru-Flow or Radial Reynolds Number	Nominal Tangential Reynolds Number at 68 F, $Re_{t,j}$	Actual Tangential Reynolds Number	Average Injection Velocity V_j-ft/sec	Nominal $\beta_{t,j}$	Actual $\beta_{t,j}$	Tangential Velocity Profile	Dye Photographs
Single Slot	0	0	57	0	120,000	105,000	3.16	∞	∞	20	8,15
" "	2.30	30	57	25	120,000	105,000	3.16	128.57	139.99	20	9,16
" "	5.00	60	57	53	120,000	105,000	3.16	64.27	66.038	21	10,17
" "	7.40	93	57	80	120,000	105,000	3.16	41.47	43.75	21	11,18
" "	9.75	125	57	110	120,000	105,000	3.16	30.85	31.52		12
" "	15.83	200	57	175	120,000	105,000	3.16	19.28	19.81		13
Four Slot	0	0	46	0	120,000	89,000	3.16	∞	∞		8,15
" "	2.30	30	46	22	120,000	89,000	3.16	128.57	138.03		9,16
" "	5.00	60	46	44	120,000	89,000	3.16	64.27	69.02		10,17
" "	7.40	93	46	69	120,000	89,000	3.16	41.47	44.01		11,18
2144 Port	0	0	40	0	120,000	80,000	3.16	∞	∞	20	8,15
" "	2.30	30	40	20	120,000	80,000	3.16	128.57	139.42	20	9,16
" "	5.00	60	40	40	120,000	80,000	3.16	64.27	69.709	21	10,17
" "	7.40	93	40	63	120,000	80,000	3.16	41.47	44.257	21	11,18
" "	9.75	125	40	84	120,000	80,000	3.16	30.85	33.193		12
" "	12.20	150	40	100	120,000	80,000	3.16	25.71	27.88		
" "	15.83	200	40	134	120,000	80,000	3.16	19.28	20.81		13
2144 Port	-0.230*	-3	47	-2.1	120,000	90,000	3.16			22	27
" "	-2.30*	-30	47	-21	120,000	90,000	3.16			22	27
" "	-5.00*	-60	47	-42	120,000	90,000	3.16			22	27
" "	-7.90*	-100	47	-71	120,000	90,000	3.16			22	27
" "	-5.00*	-60	47	-42	240,000	180,000	6.32				
" "	-5.00*	-60	47	-42	360,000	270,000	9.48				

* Fluid injection through centerline porous tube (see APPENDIX)

FIG. 1

GEOMETRY OF TYPICAL VORTEX TUBE EMPLOYED IN TESTS

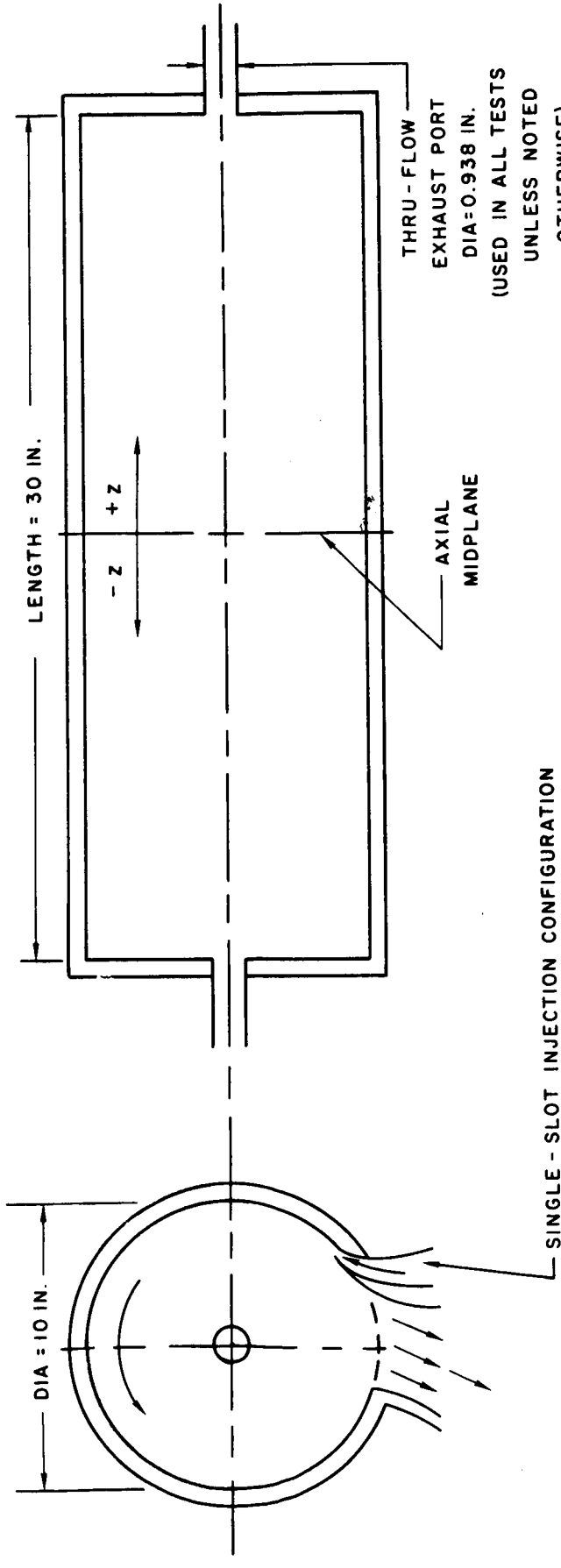

FIG. 2

DETAILS OF INJECTION CONFIGURATIONS

SINGLE - SLOT INJECTION

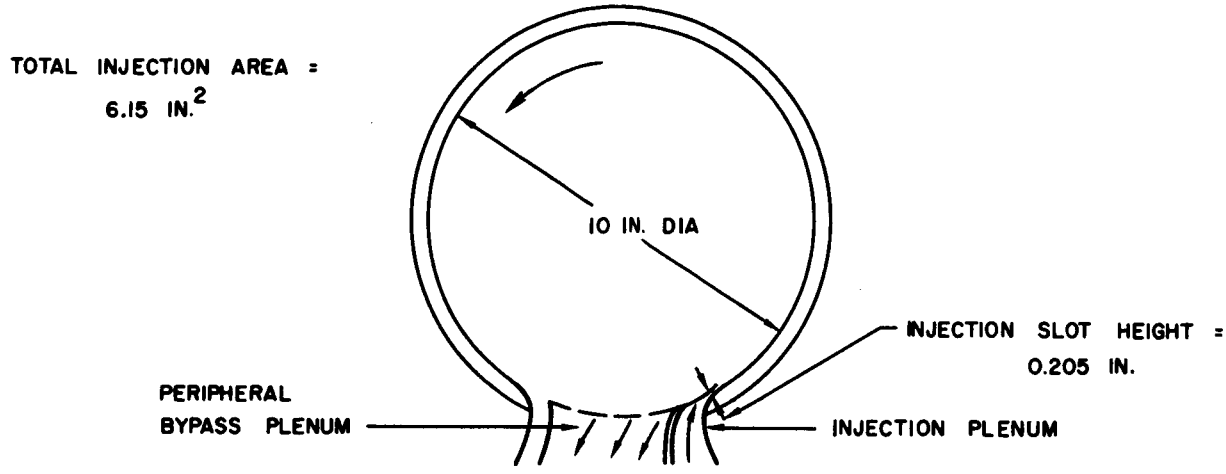

FOUR - SLOT INJECTION

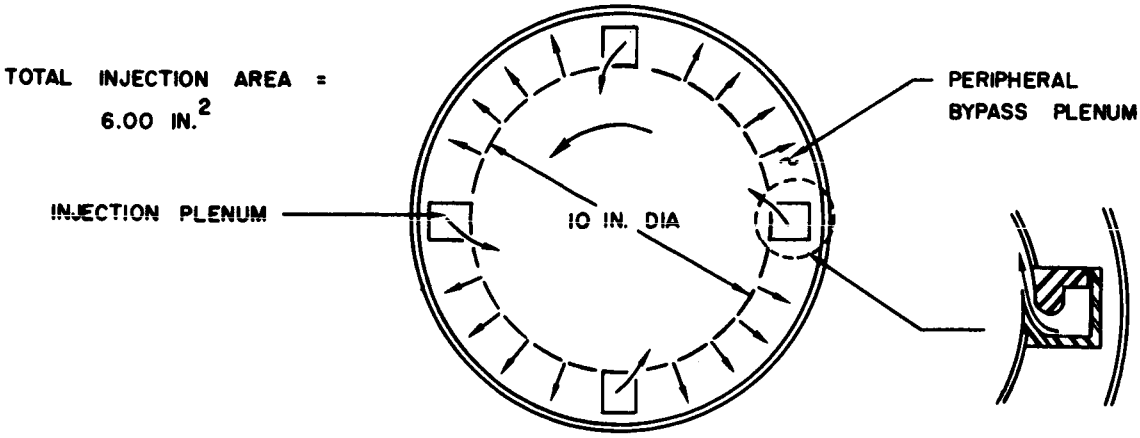

2144 - PORT INJECTION

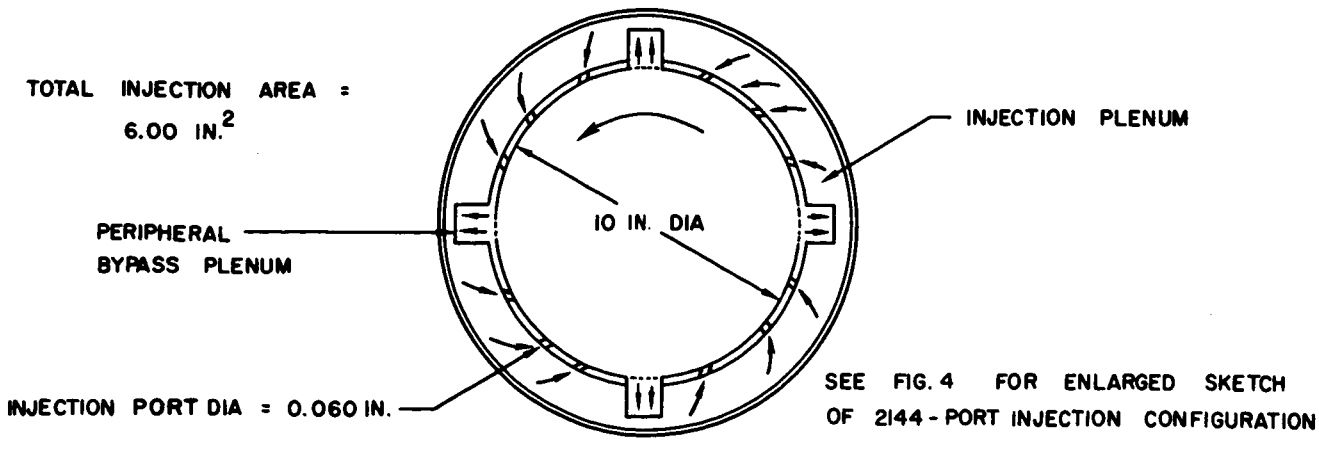

SEE FIG. 4 FOR ENLARGED SKETCH OF 2144 - PORT INJECTION CONFIGURATION

FIG. 3

PHOTOGRAPHS OF SINGLE-SLOT-INJECTION AND 2144-PORT-INJECTION VORTEX TUBES

SINGLE-SLOT INJECTION

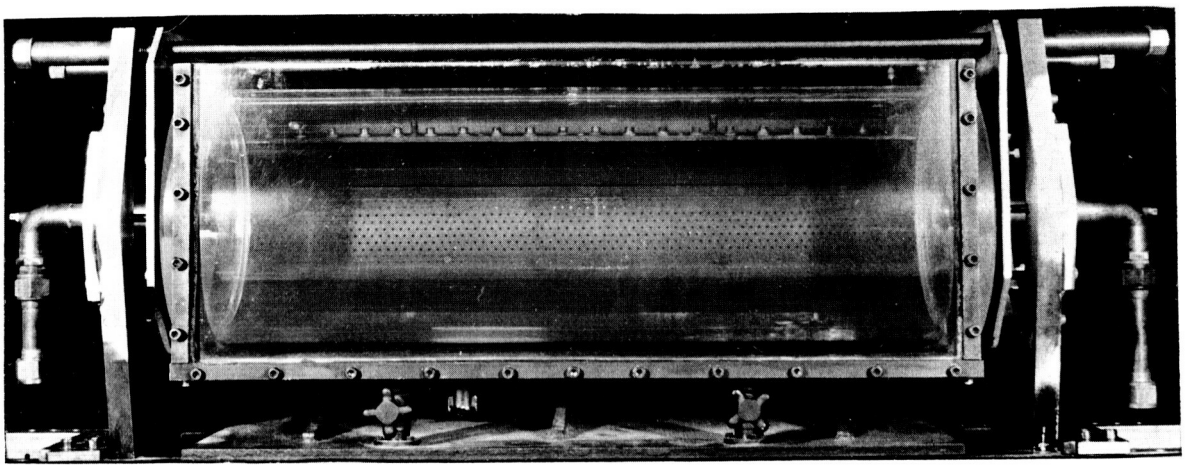

2144-PORT INJECTION

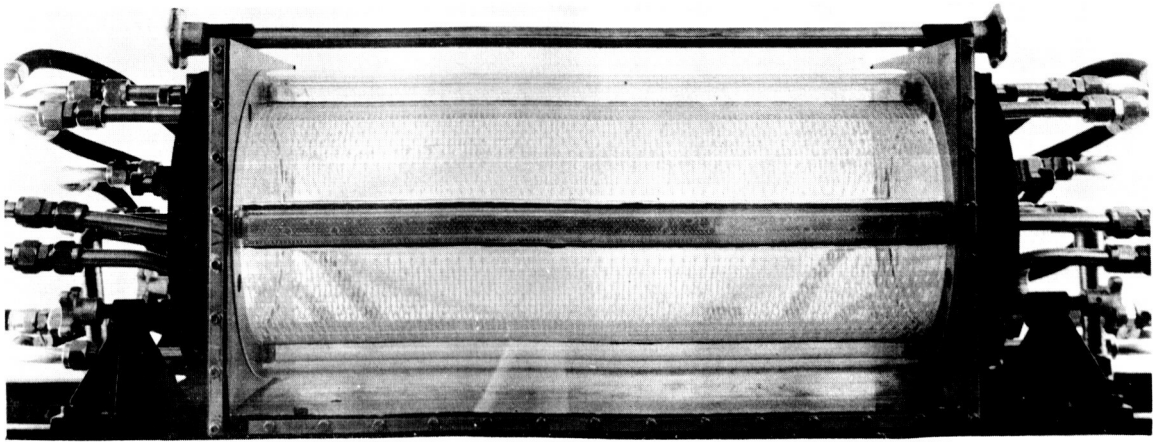

SKETCH OF ONE QUADRANT OF 2144-PORT INJECTION CONFIGURATION

FULL SCALE

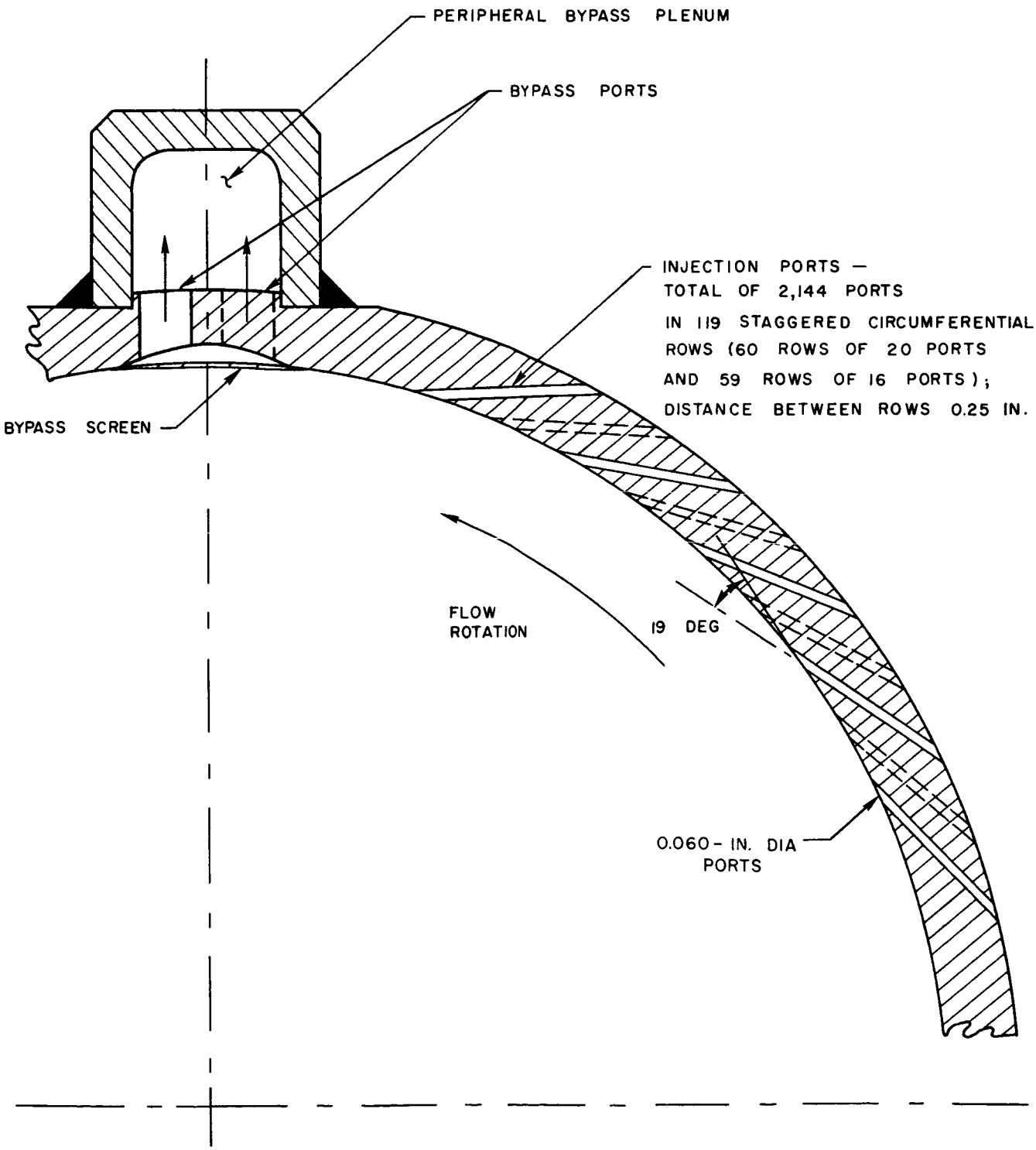

OPTICAL SYSTEM USED TO OBTAIN DYE AND PARTICLE-TRACE PHOTOGRAPHS

NOTE: FOR DYE PHOTOGRAPHS THROUGH SIDE OF VORTEX TUBE, LOCATIONS OF CAMERA AND LIGHT SOURCE WERE INTERCHANGED

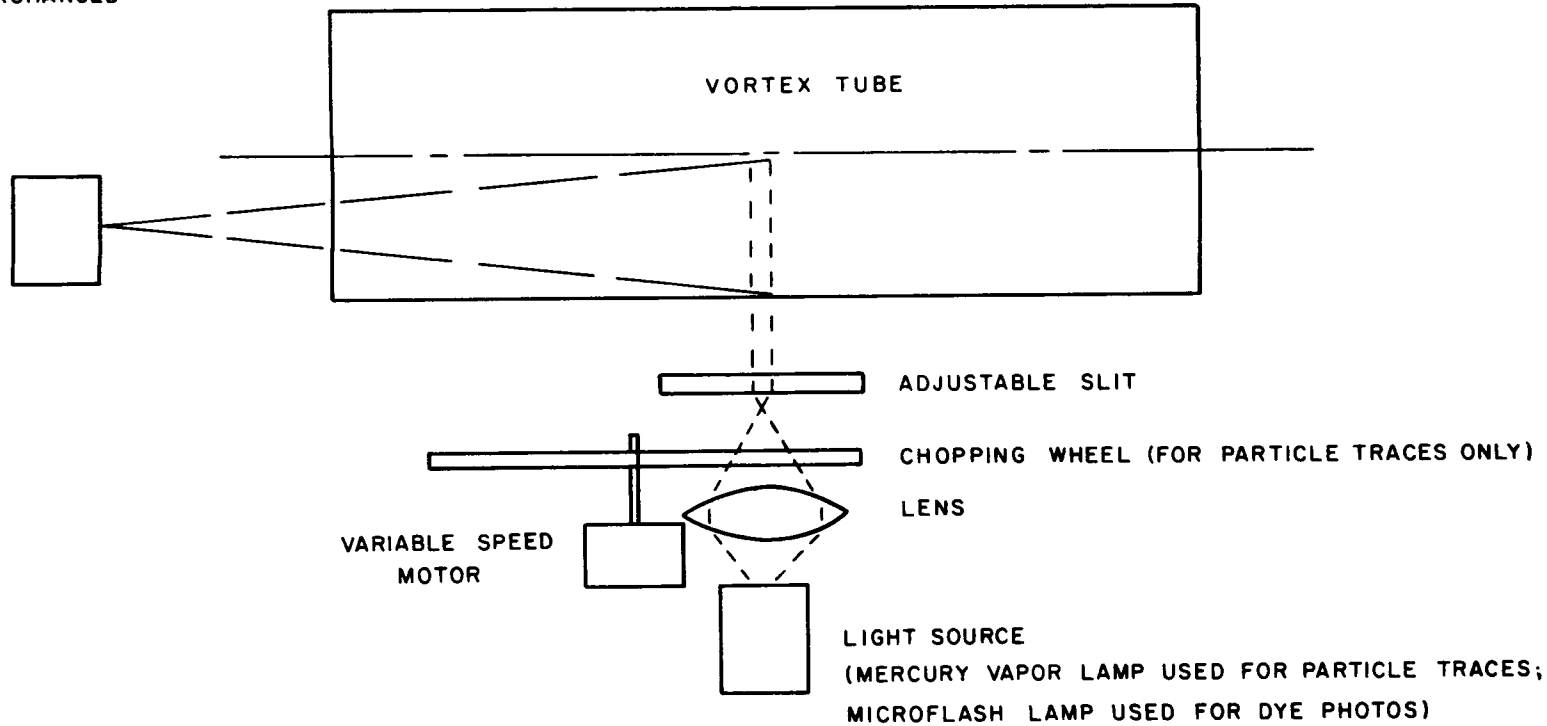

FIG. 5

FIG. 6

TYPICAL PARTICLE-TRACE PHOTOGRAPH

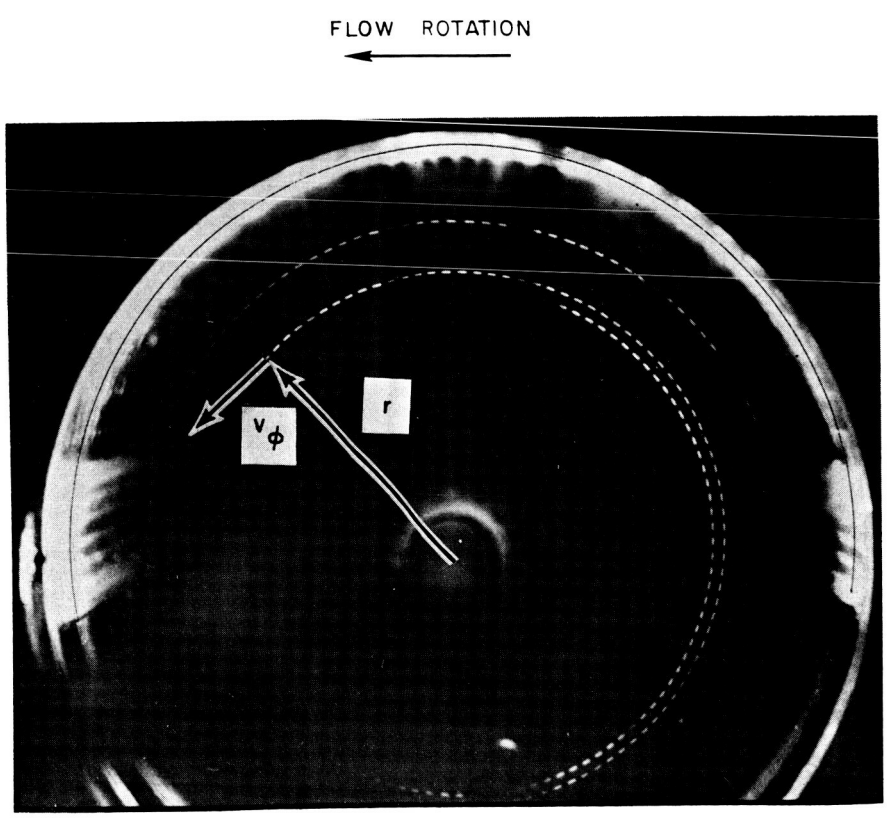

TYPICAL TANGENTIAL VELOCITY PROFILE SHOWING SCATTER OF PARTICLE-TRACE DATA

$Re_{t,j}$ = 120,000 v_j = 3.16 FT/SEC

$Re_{r,t}$ = 30

2144 - PORT INJECTION

SEE FIG. 2 FOR DETAILS OF INJECTION CONFIGURATION

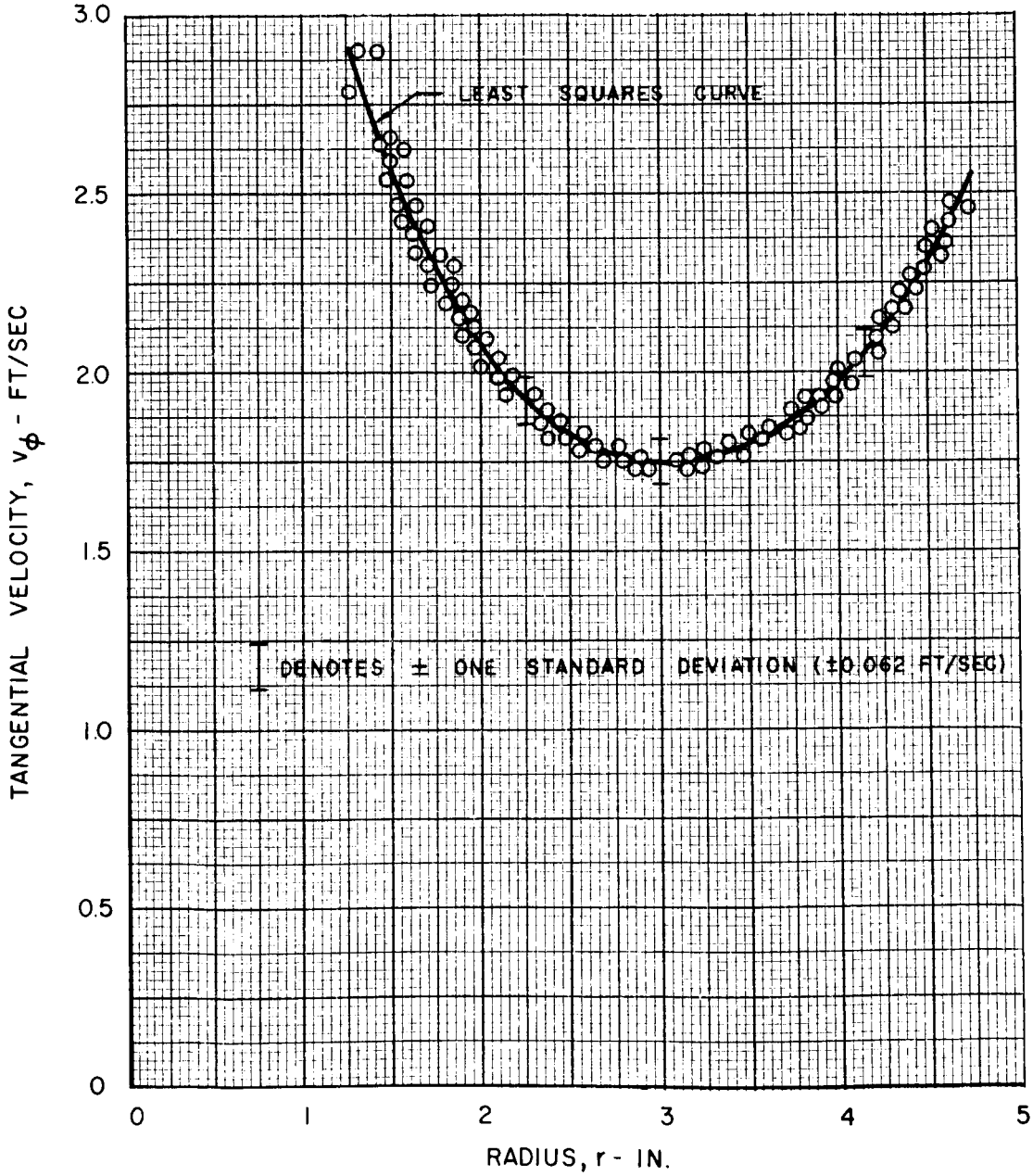

FIG. 8

MICROFLASH PHOTOGRAPHS OF DYE PATTERNS FOR ALL THREE INJECTION CONFIGURATIONS AT THRU-FLOW REYNOLDS NUMBER OF 0

$Re_{t,j} = 120{,}000$

SEE FIG. 2 FOR DETAILS OF INJECTION CONFIGURATIONS

DYE INJECTION THROUGH PERIPHERAL WALL AT AXIAL MIDPLANE

FLOW ROTATION

SINGLE - SLOT INJECTION

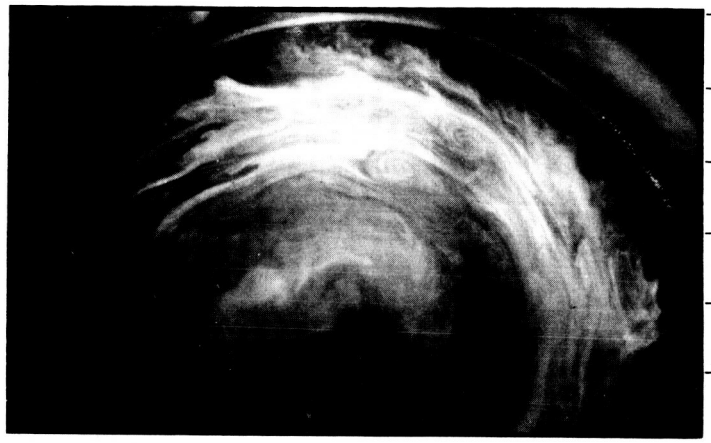

FOUR - SLOT INJECTION

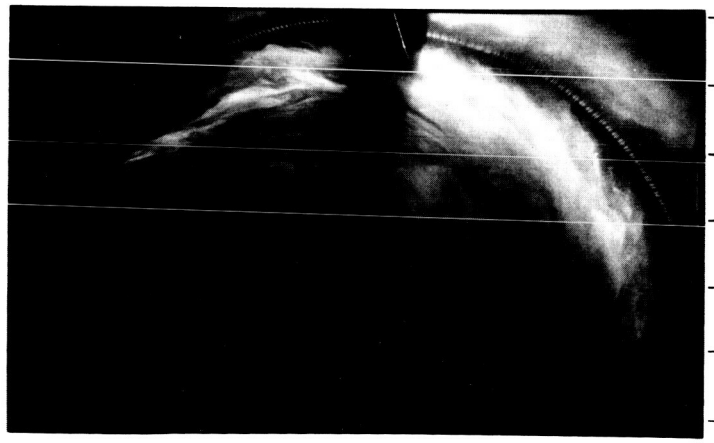

2144 - PORT INJECTION

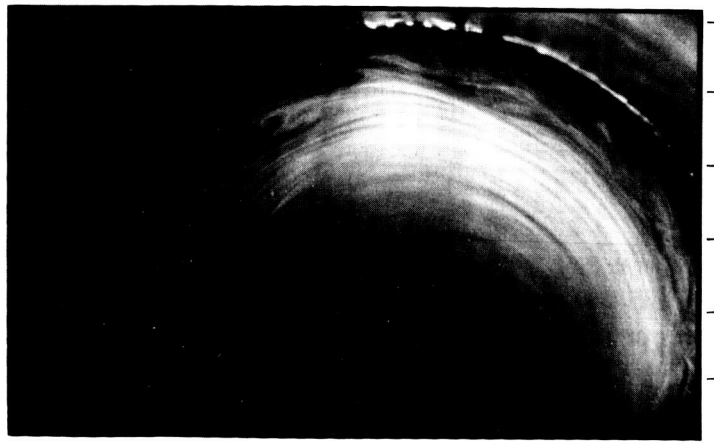

FIG. 9

MICROFLASH PHOTOGRAPHS OF DYE PATTERNS FOR ALL THREE INJECTION CONFIGURATIONS AT THRU-FLOW REYNOLDS NUMBER OF 30

$Re_{t,j}$ 120,000

SEE FIG. 2 FOR DETAILS OF INJECTION CONFIGURATIONS
DYE INJECTION THROUGH PERIPHERAL WALL AT AXIAL MIDPLANE

FLOW ROTATION

SINGLE - SLOT INJECTION

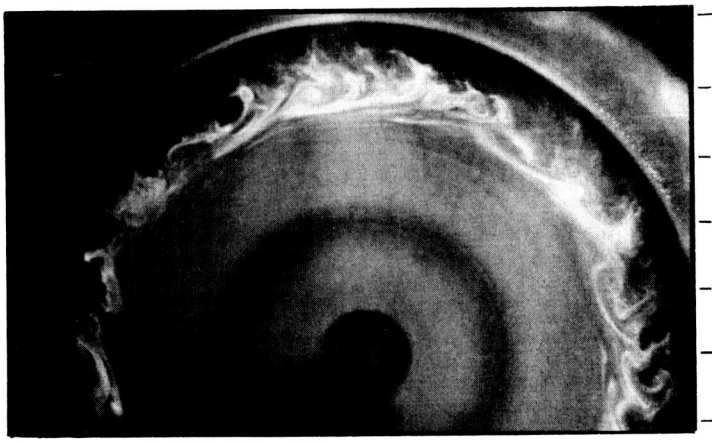

FOUR - SLOT INJECTION

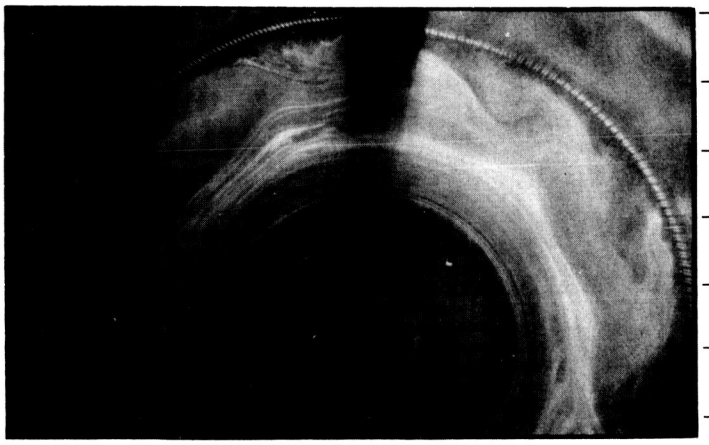

2144 - PORT INJECTION

FIG. 10

MICROFLASH PHOTOGRAPHS OF DYE PATTERNS FOR ALL THREE INJECTION CONFIGURATIONS AT THRU-FLOW REYNOLDS NUMBER OF 60

$Re_{t,j} = 120{,}000$

SEE FIG. 2 FOR DETAILS OF INJECTION CONFIGURATIONS

DYE INJECTION THROUGH PERIPHERAL WALL AT AXIAL MIDPLANE

FLOW ROTATION ←

SINGLE-SLOT INJECTION

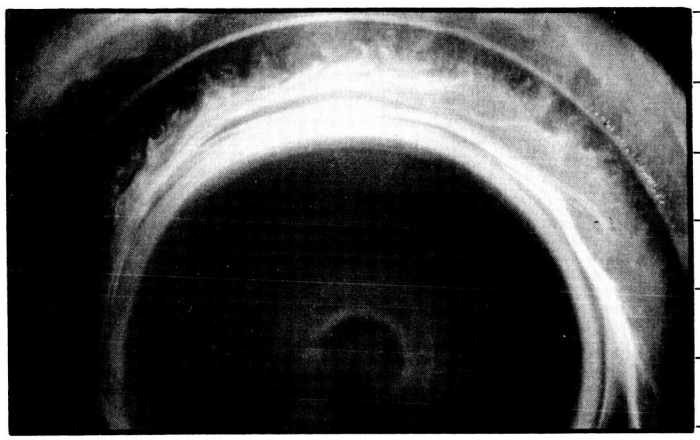

FOUR-SLOT INJECTION

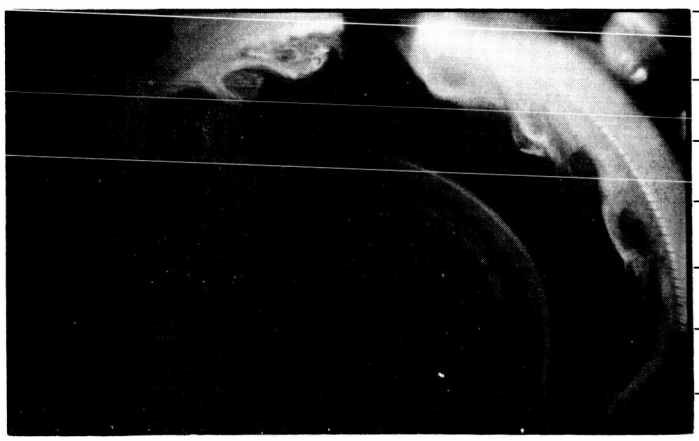

2144-PORT INJECTION

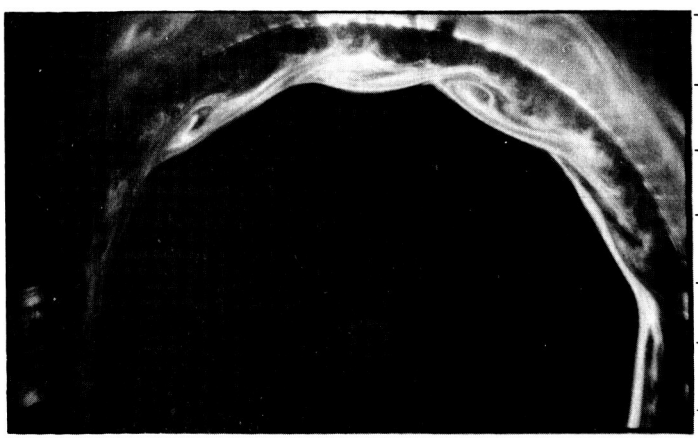

MICROFLASH PHOTOGRAPHS OF DYE PATTERNS FOR ALL THREE INJECTION CONFIGURATIONS AT THRU-FLOW REYNOLDS NUMBER OF 93

$Re_{t,j} = 120{,}000$

SEE FIG. 2 FOR DETAILS OF INJECTION CONFIGURATIONS

DYE INJECTION THROUGH PERIPHERAL WALL AT AXIAL MIDPLANE

FLOW ROTATION ←

SINGLE-SLOT INJECTION

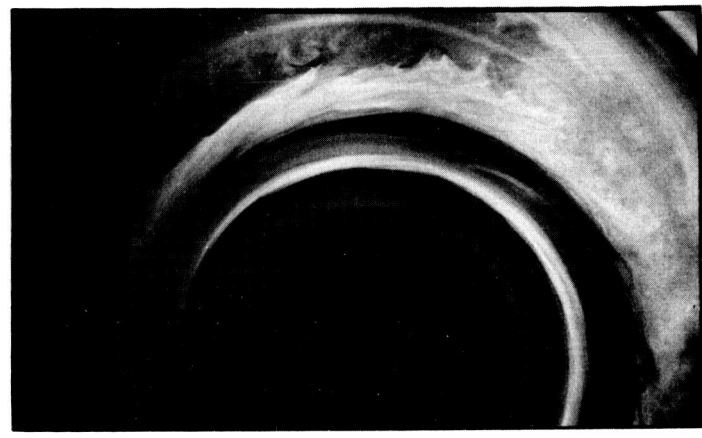

FOUR-SLOT INJECTION

2144-PORT INJECTION

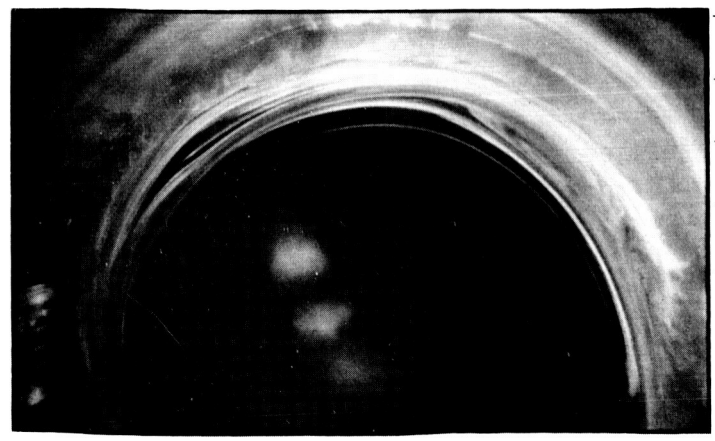

FIG. 12

MICROFLASH PHOTOGRAPHS OF DYE PATTERNS FOR SINGLE-SLOT AND 2144-PORT INJECTION CONFIGURATIONS AT THRU-FLOW REYNOLDS NUMBER OF 125

$Re_{t,j}$ = 120,000

SEE FIG. 2 FOR DETAILS OF INJECTION CONFIGURATIONS

DYE INJECTION THROUGH PERIPHERAL WALL AT AXIAL MIDPLANE

FLOW ROTATION

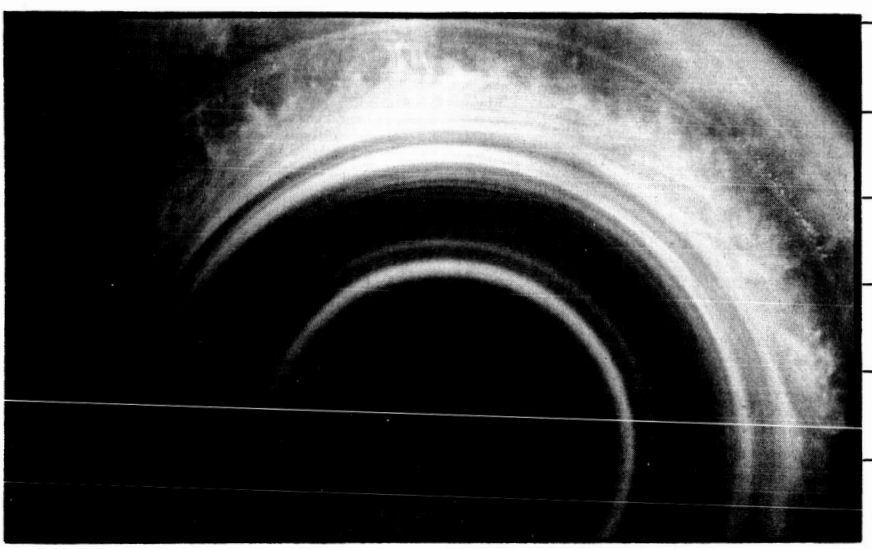

SINGLE - SLOT INJECTION

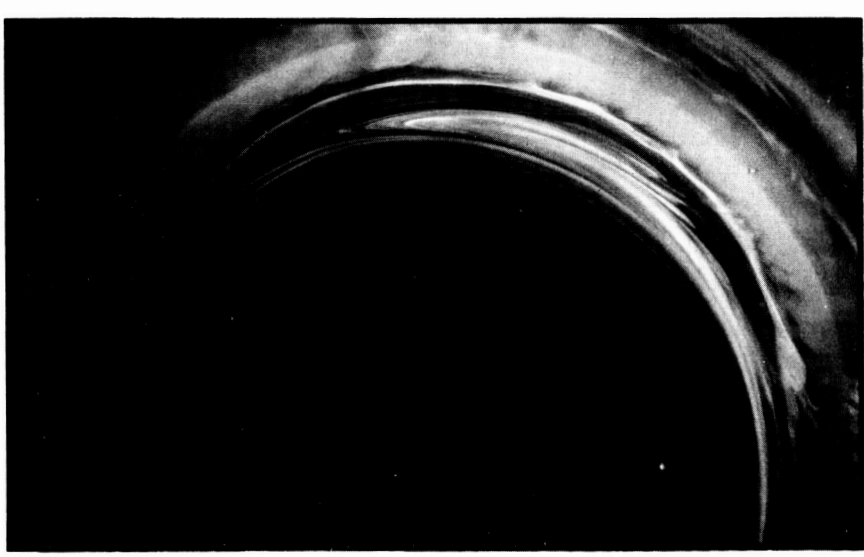

2144 - PORT INJECTION

FIG. 13

MICROFLASH PHOTOGRAPHS OF DYE PATTERNS FOR SINGLE-SLOT AND 2144-PORT INJECTION CONFIGURATIONS AT THRU-FLOW REYNOLDS NUMBER OF 200

$Re_{t,j}$ = 120,000

SEE FIG. 2 FOR DETAILS OF INJECTION CONFIGURATIONS

DYE INJECTION THROUGH PERIPHERAL WALL AT AXIAL MIDPLANE

FLOW ROTATION

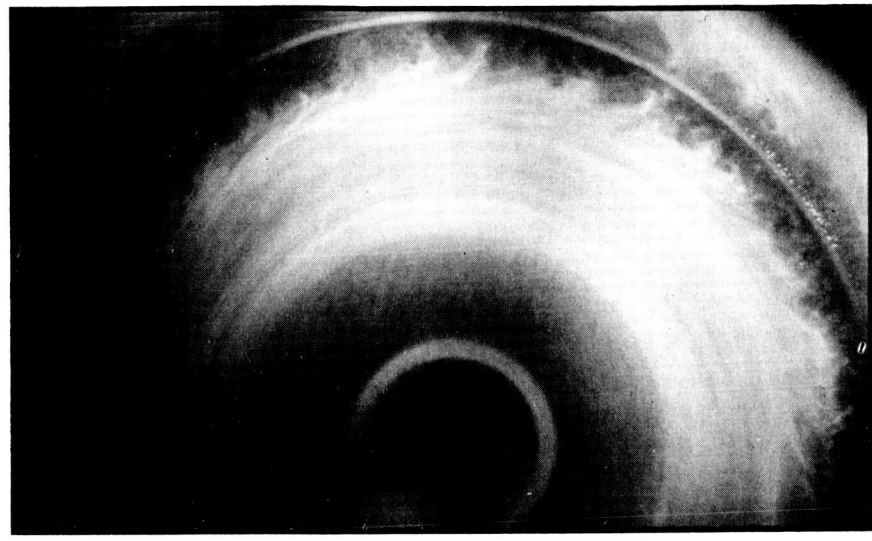

SINGLE - SLOT INJECTION

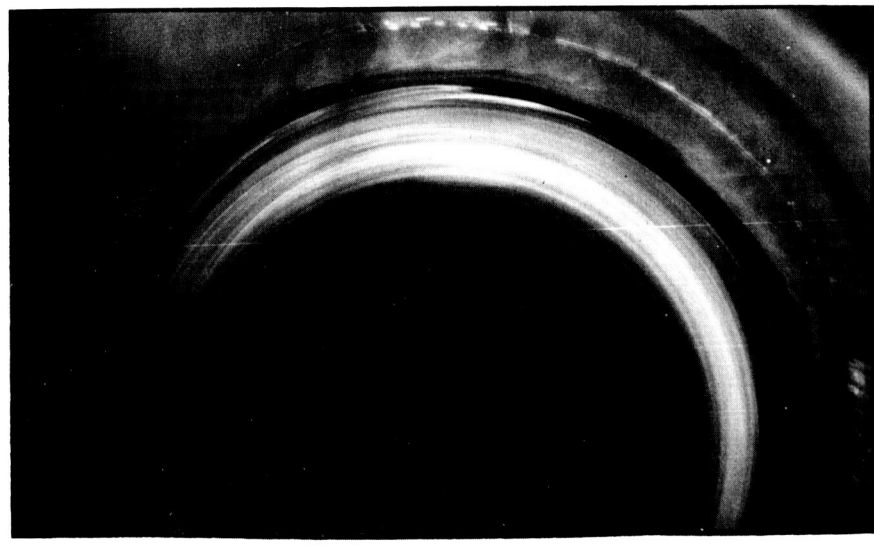

2144 - PORT INJECTION

FIG. 14

TURBULENT ENERGY SPECTRA FOR SINGLE-SLOT AND 2144-PORT INJECTION CONFIGURATION AT A RADIUS OF 4.75 IN. AND THRU-FLOW REYNOLDS NUMBER OF 100

$Re_{t,j}$ = 190,000 v_j = 76 FT/SEC $\beta_{t,j}$ = 56

AIR VORTEX DATA FROM REF. 4

SEE FIG. 2 FOR DETAILS OF INJECTION CONFIGURATIONS

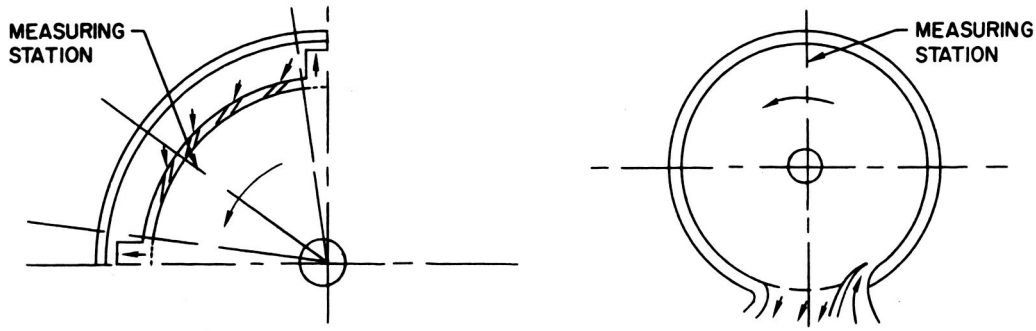

2144 - PORT INJECTION

SINGLE-SLOT INJECTION

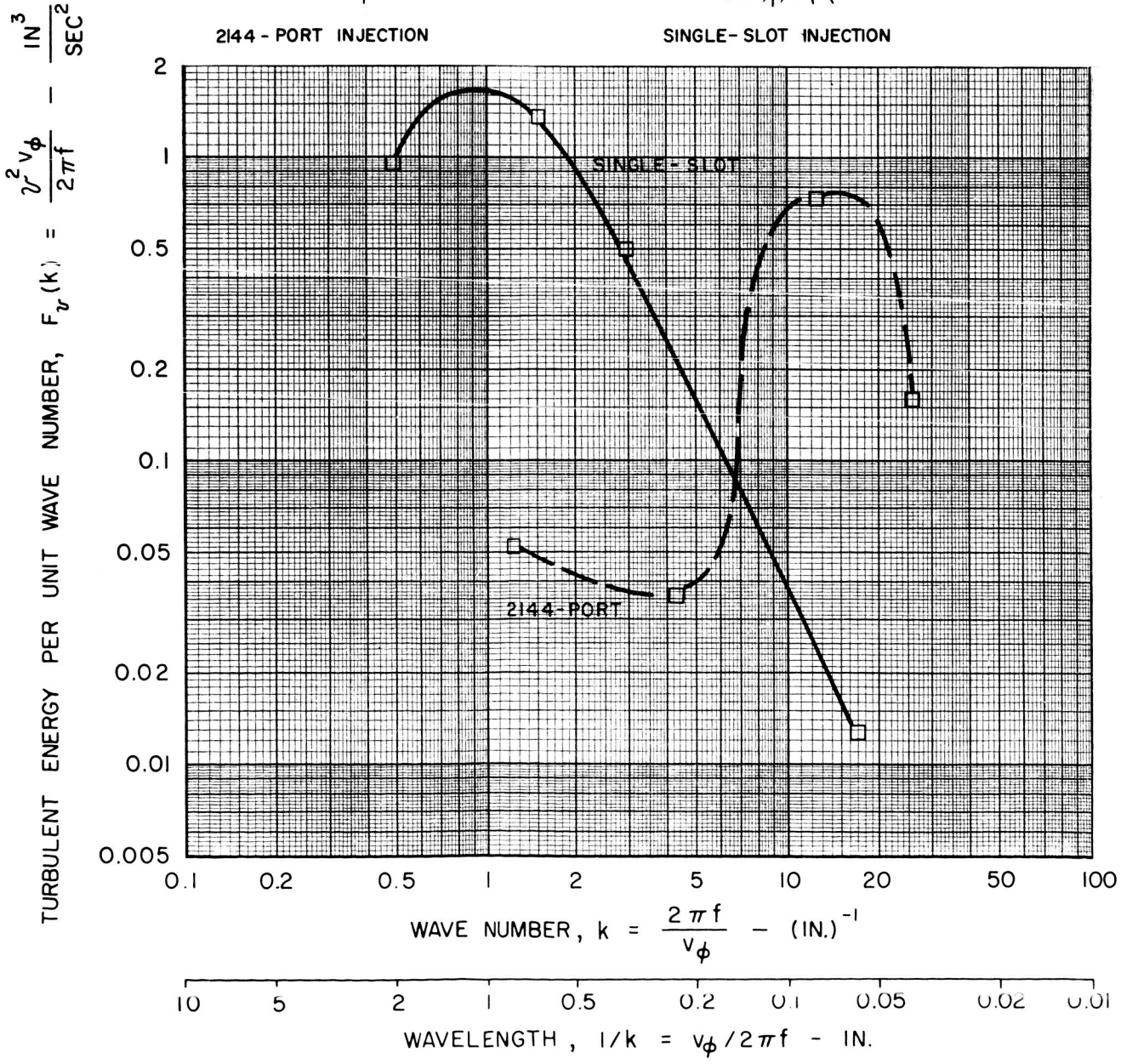

FIG. 15

PHOTOGRAPHS OF DYE PATTERNS FOR ALL THREE INJECTION CONFIGURATIONS AT THRU-FLOW REYNOLDS NUMBER OF 0

$Re_{t,j}$ = 120,000

SEE FIG. 2 FOR DETAILS OF INJECTION CONFIGURATIONS

PHOTOGRAPHS TAKEN AT INDICATED TIMES
AFTER CESSATION OF DYE INJECTION THROUGH END WALLS

SINGLE-SLOT INJECTION - 0.75 MIN

FOUR-SLOT INJECTION - 1.00 MIN

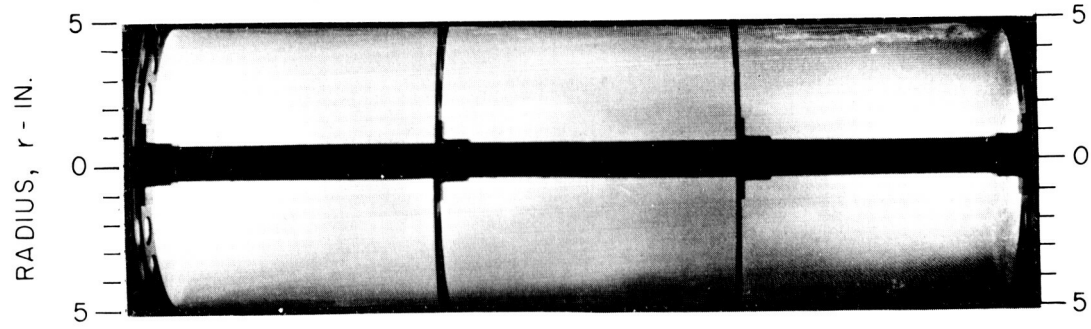

2144 - PORT INJECTION - 0.75 MIN

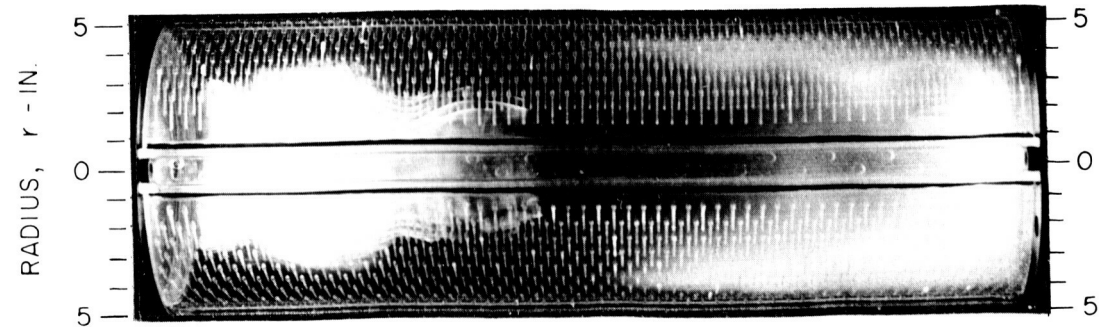

FIG. 16

PHOTOGRAPHS OF DYE PATTERNS FOR ALL THREE INJECTION CONFIGURATIONS AT THRU-FLOW REYNOLDS NUMBER OF 30

$Re_{t,j}$ = 120,000

SEE FIG. 2 FOR DETAILS OF INJECTION CONFIGURATIONS

PHOTOGRAPHS TAKEN AT INDICATED TIMES
AFTER CESSATION OF DYE INJECTION THROUGH END WALLS

SINGLE-SLOT INJECTION - 6.0 MIN

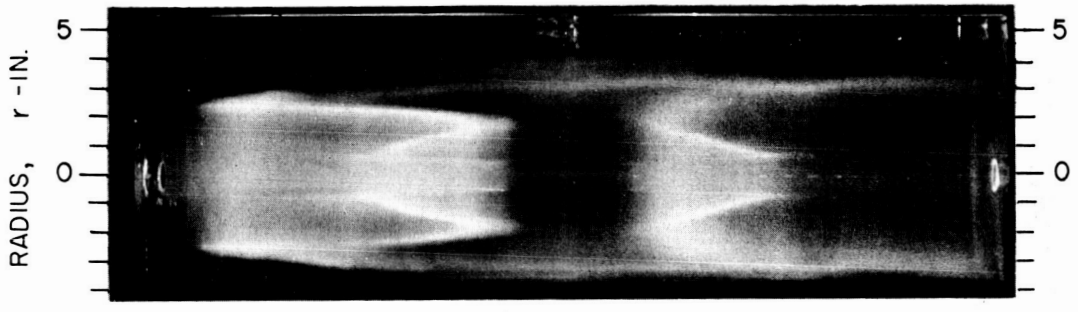

FOUR-SLOT INJECTION - 7.0 MIN

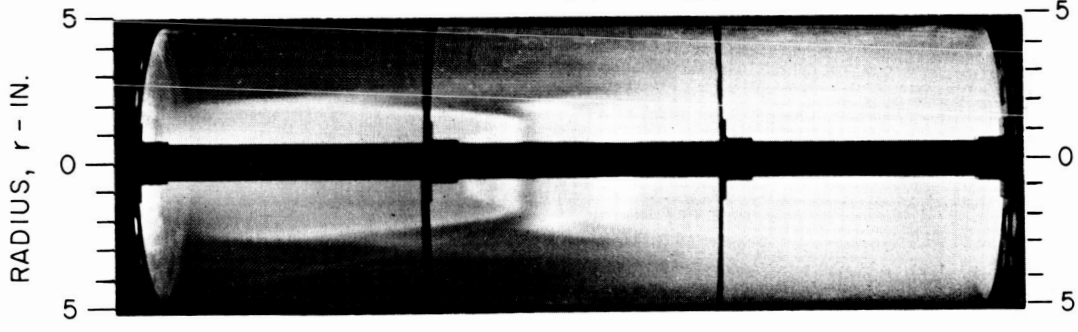

2144-PORT INJECTION - 7.0 MIN

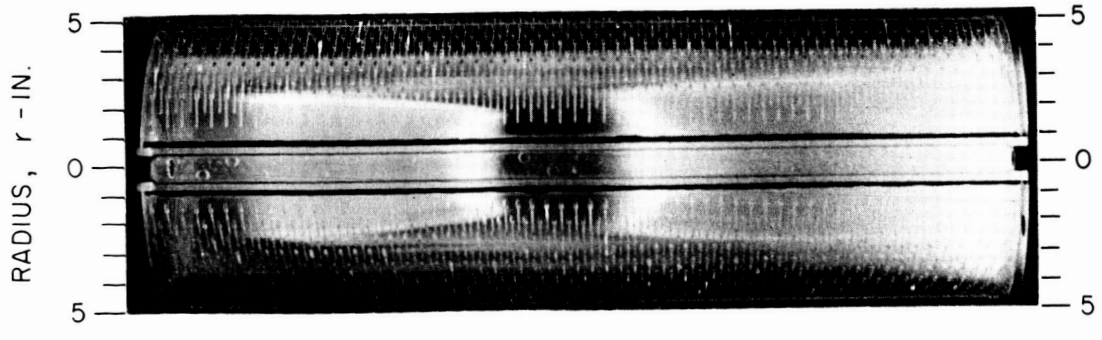

FIG. 17

PHOTOGRAPHS OF DYE PATTERNS FOR ALL THREE INJECTION CONFIGURATIONS AT THRU-FLOW REYNOLDS NUMBER OF 60

$Re_{t,j}$ = 120,000

SEE FIG. 2 FOR DETAILS OF INJECTION CONFIGURATIONS

PHOTOGRAPHS TAKEN AT INDICATED TIMES
AFTER CESSATION OF DYE INJECTION THROUGH END WALLS

SINGLE-SLOT INJECTION - 5.75 MIN.

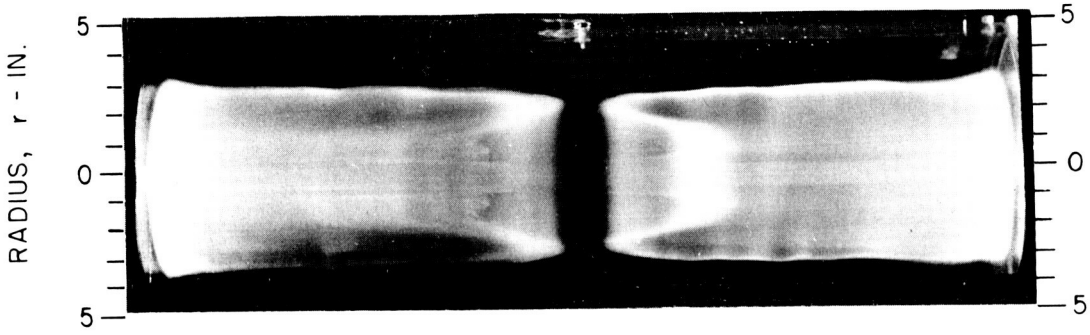

FOUR-SLOT INJECTION - 6.00 MIN.

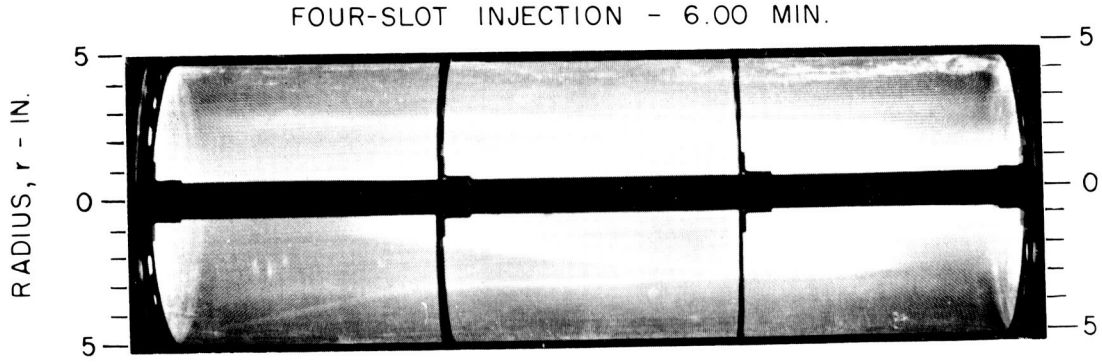

2144-PORT INJECTION - 6.00 MIN.

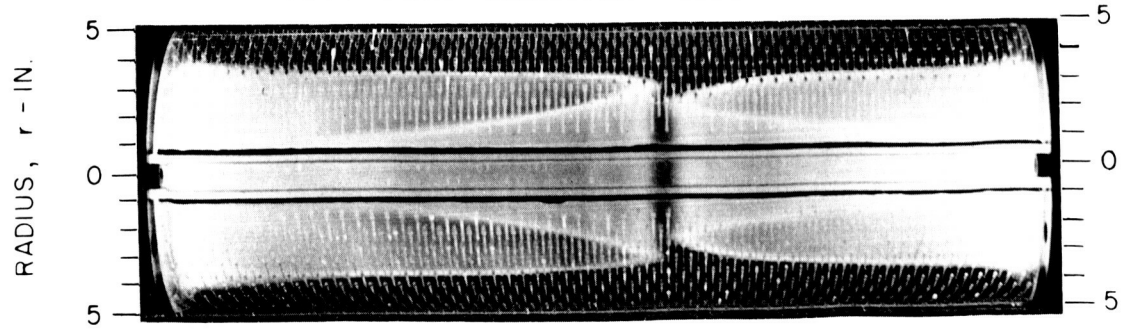

FIG. 18

PHOTOGRAPHS OF DYE PATTERNS FOR ALL THREE INJECTION CONFIGURATIONS AT THRU-FLOW REYNOLDS NUMBER OF 93

$Re_{t,j}$ = 120,000

SEE FIG. 2 FOR DETAILS OF INJECTION CONFIGURATIONS

PHOTOGRAPHS TAKEN AT INDICATED TIMES
AFTER CESSATION OF DYE INJECTION THROUGH END WALLS

SINGLE-SLOT INJECTION - 3.0 MIN

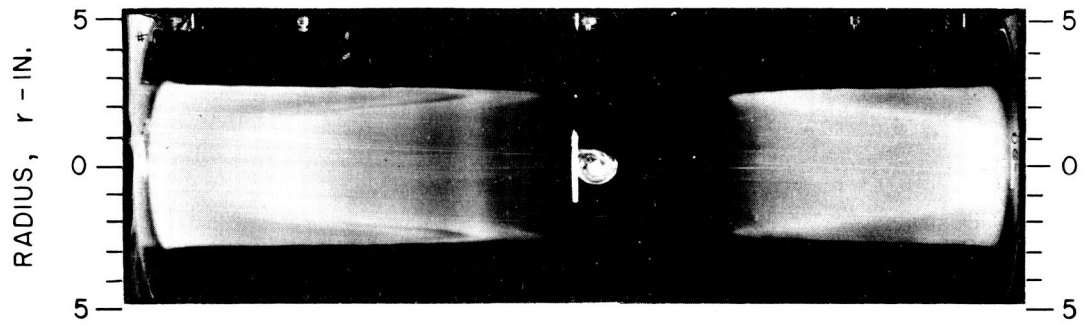

FOUR-SLOT INJECTION - 3.0 MIN

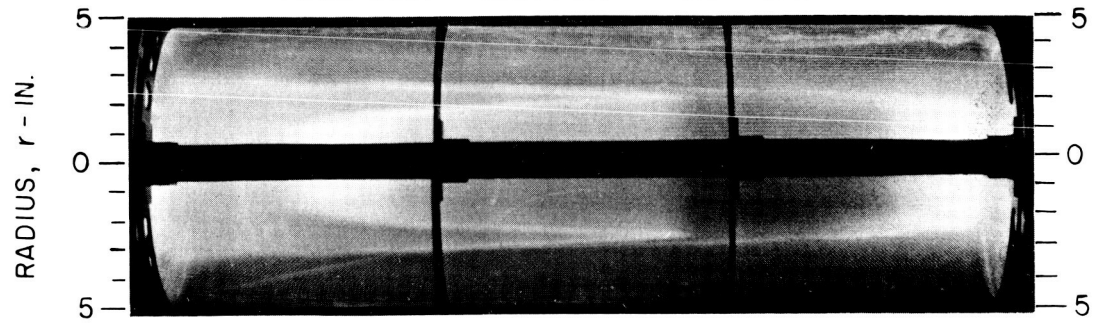

2144 - PORT INJECTION - 3.0 MIN

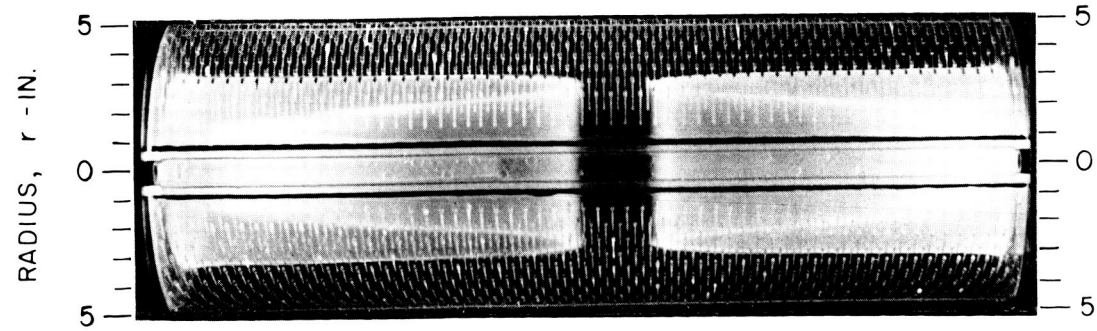

FIG. 19

EFFECT OF THRU-FLOW RATE ON RADIUS OF RADIAL STAGNATION SURFACE FOR ALL THREE INJECTION CONFIGURATIONS

$Re_{t,j}$ = 120,000

OUTER EDGE OF DYE ANNULUS MOVED RADIALLY INWARD WITH TIME FOR $Re_{r,t}$ GREATER THAN VALUES NOTED BY ⌐*

SEE FIG. 2 FOR DETAILS OF INJECTION CONFIGURATIONS

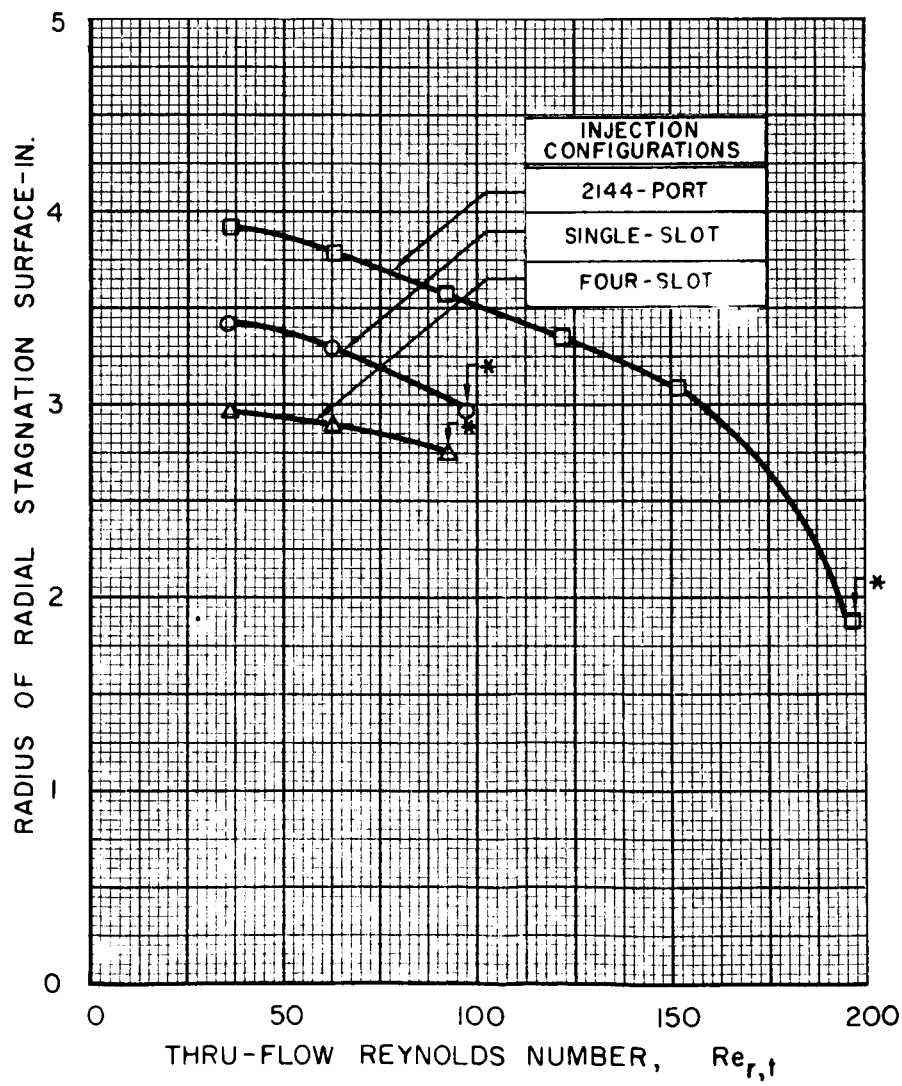

TANGENTIAL VELOCITY PROFILES FOR SINGLE-SLOT AND 2144-PORT INJECTION CONFIGURATIONS AT THRU-FLOW REYNOLDS NUMBERS OF 0 AND 30

$Re_{t,j}$ = 120,000

V_j = 3.16 FT/SEC

SEE FIG. 2 FOR DETAILS OF INJECTION CONFIGURATIONS

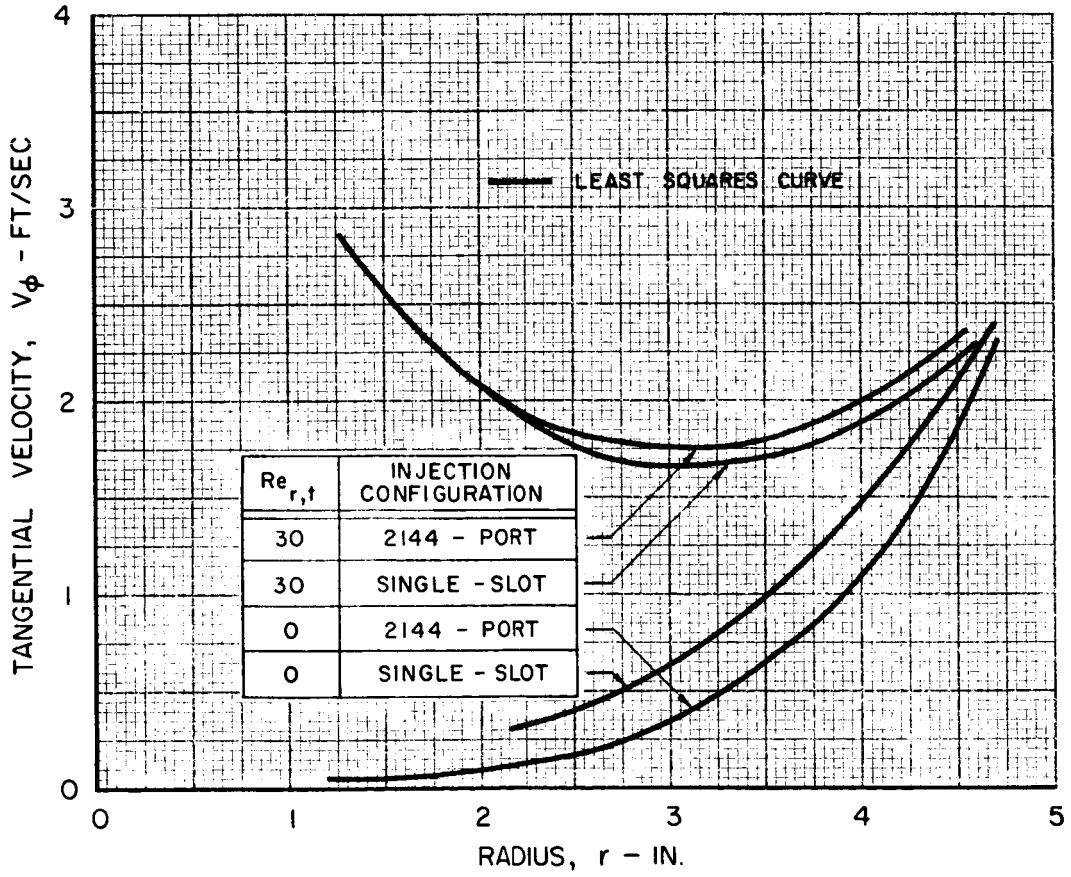

FIG. 21

TANGENTIAL VELOCITY PROFILES FOR SINGLE-SLOT AND 2144-PORT INJECTION CONFIGURATIONS AT THRU-FLOW REYNOLDS NUMBERS OF 60 AND 93

$Re_{t,j}$ = 120,000

V_j = 3.16 FT/SEC

SEE FIG. 2 FOR DETAILS OF INJECTION CONFIGURATIONS

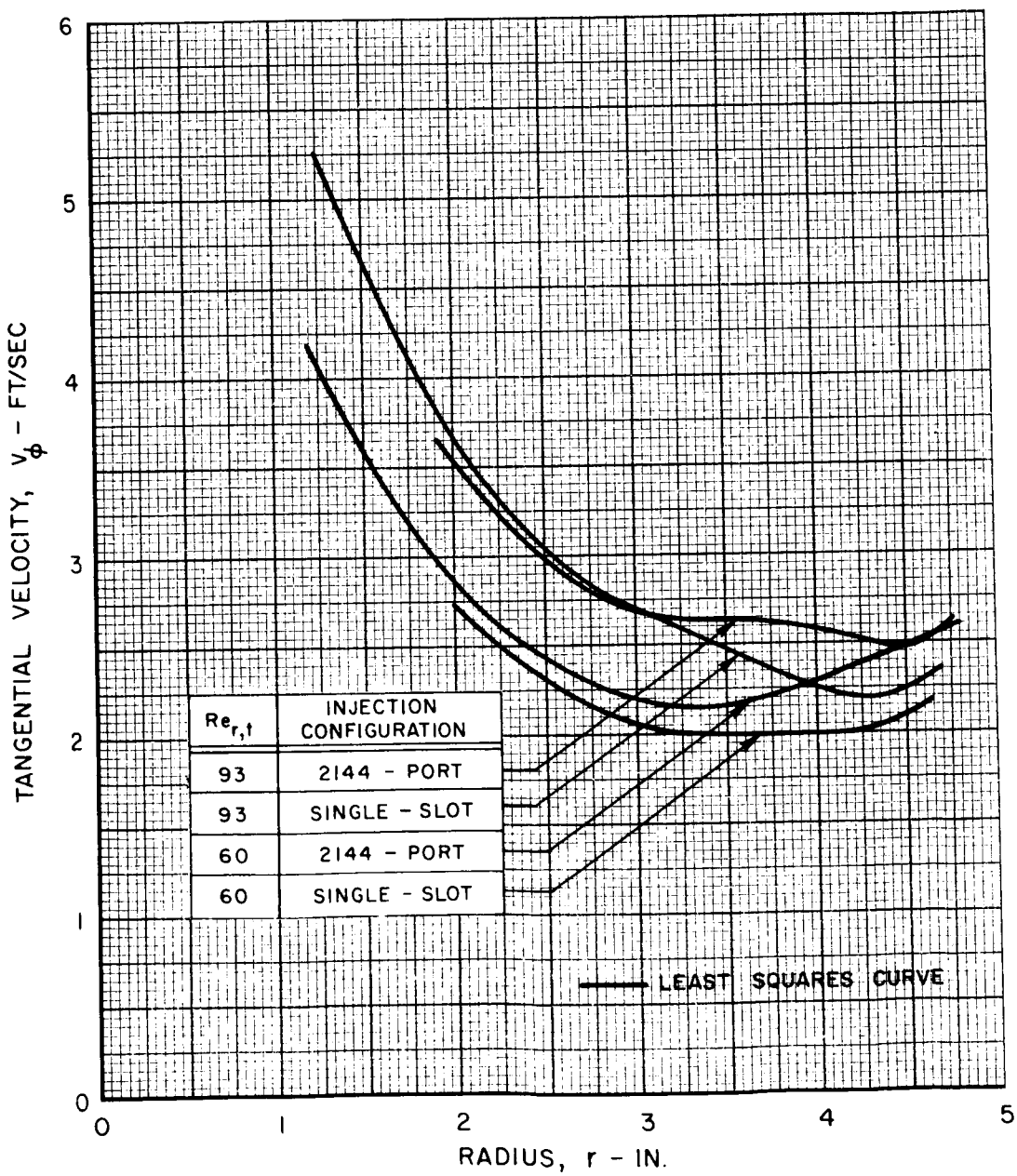

EFFECT OF OUTFLOW RADIAL REYNOLDS NUMBER ON TANGENTIAL VELOCITY PROFILES WITH FLUID INJECTION THROUGH CENTERLINE POROUS TUBE

$Re_{t,j}$ = 120,000 V_j = 3.16 FT/SEC

2144 - PORT INJECTION

SEE FIG. 2 FOR DETAILS OF INJECTION CONFIGURATION

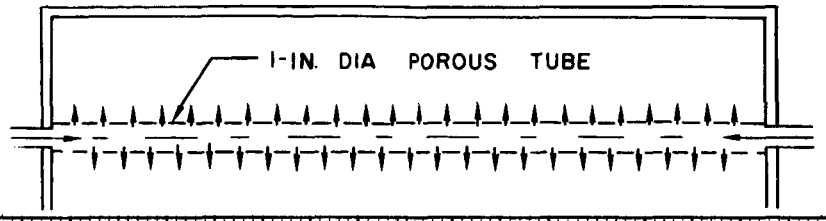

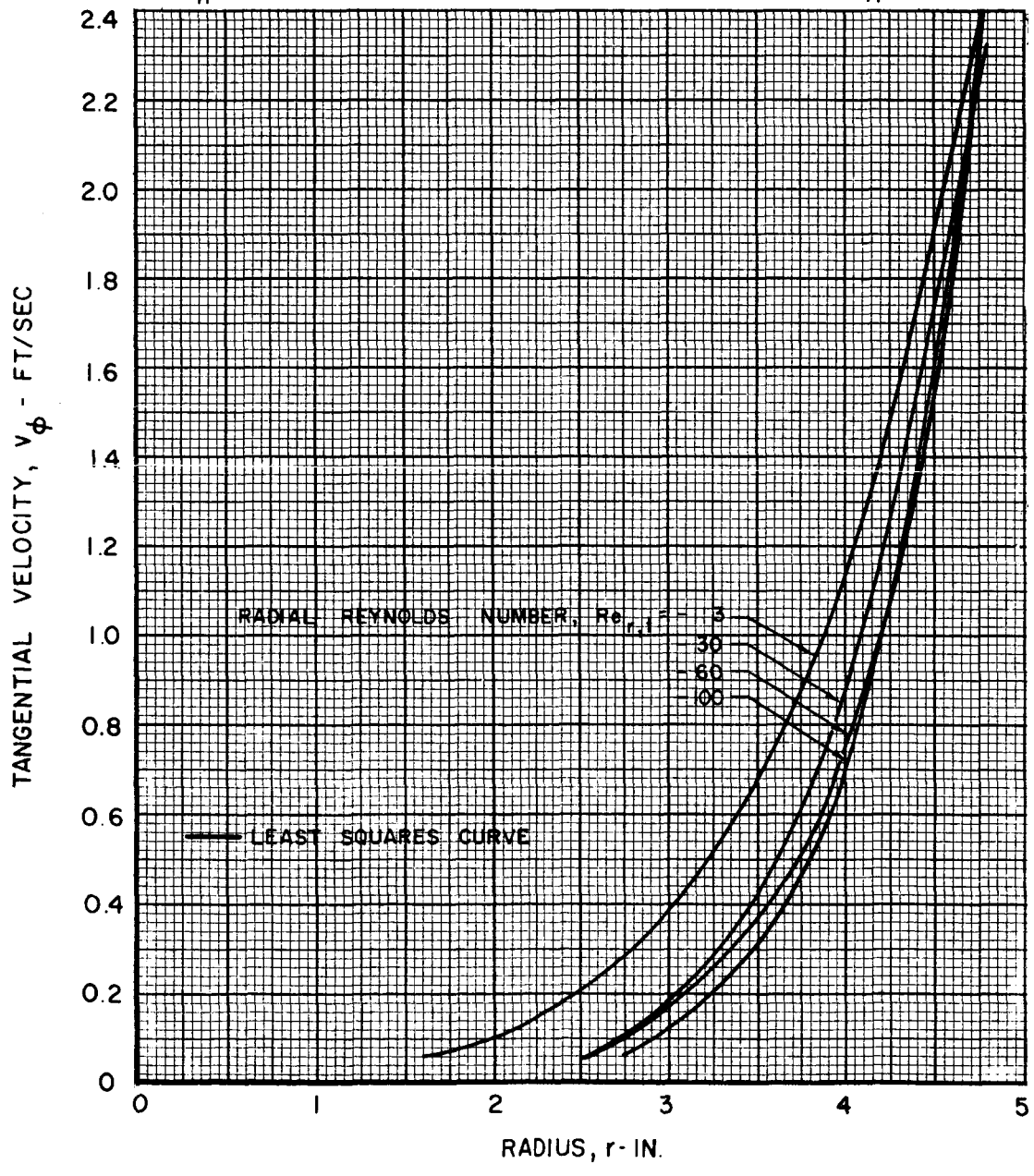

FIG. 23

TYPICAL CIRCULATION PROFILE WITH FLUID INJECTION THROUGH CENTERLINE POROUS TUBE SHOWING SCATTER OF PARTICLE-TRACE DATA

$Re_{t,j}$ = 120,000 v_j = 3.16 FT/SEC $Re_{r,t}$ = −60

2144-PORT INJECTION

SEE FIG. 2 FOR DETAILS OF INJECTION CONFIGURATION

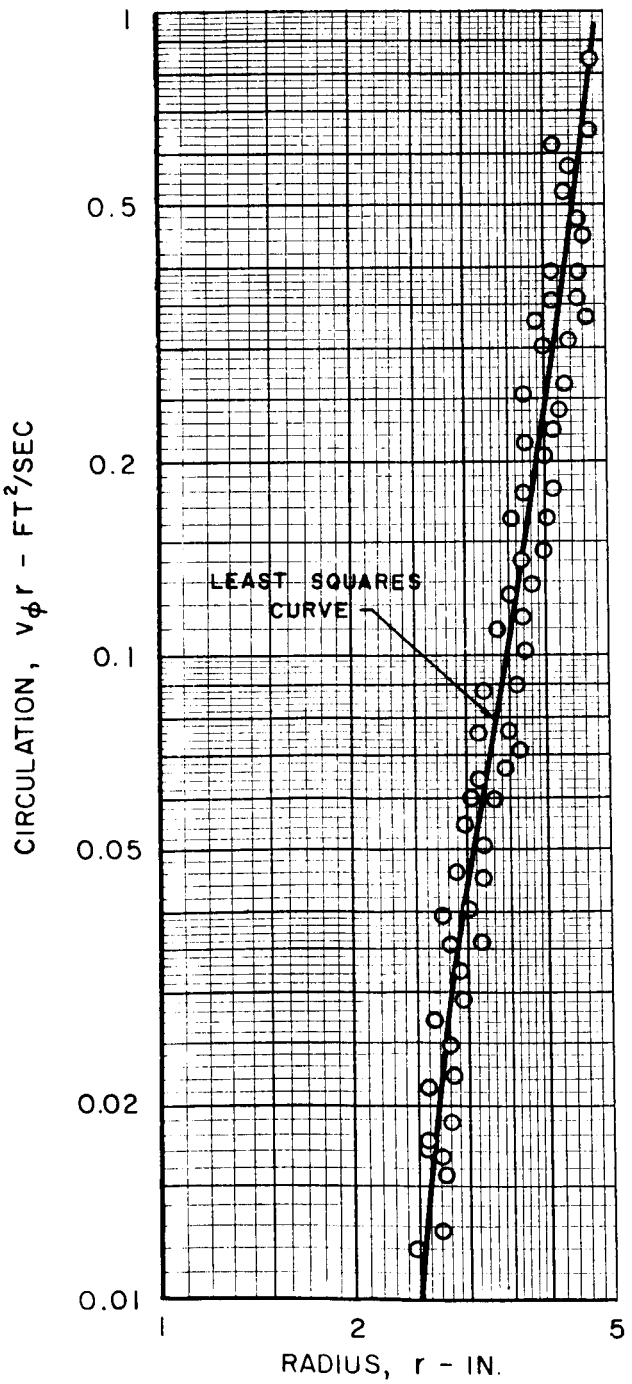

FIG. 24

EFFECT OF OUTFLOW RADIAL REYNOLDS NUMBER ON CIRCULATION PROFILES WITH FLUID INJECTION THROUGH CENTERLINE POROUS TUBE

$Re_{t,j}$ = 120,000 $v_j r_1$ = 1.3167 FT^2/SEC v_j = 3.16 FT/SEC

2144 - PORT INJECTION

SEE FIG.2 FOR DETAILS OF INJECTION CONFIGURATION

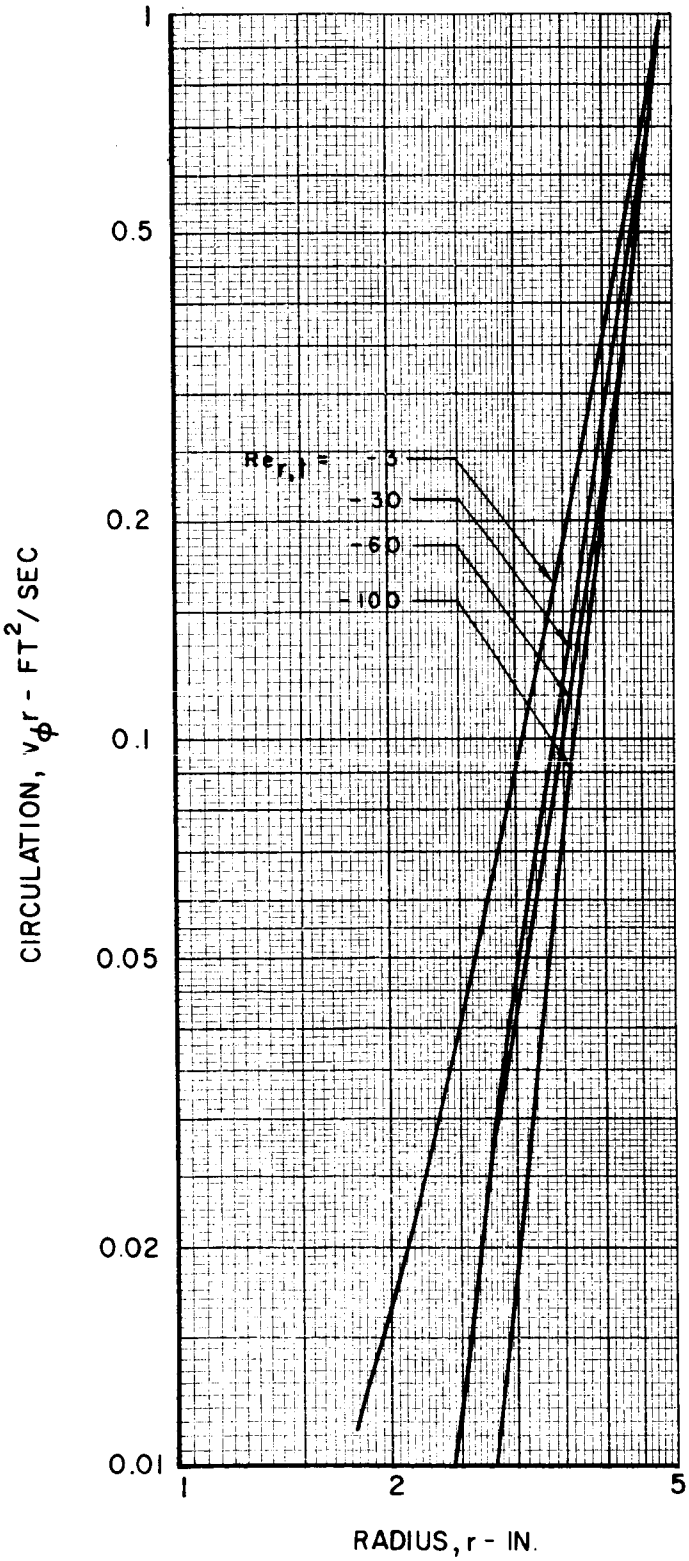

FIG. 25

COMPARISON OF THEORETICAL AND EXPERIMENTAL VARIATIONS OF n_r WITH OUTFLOW RADIAL REYNOLDS NUMBER

$$v_\phi r \propto r^{n_r}$$

LAMINAR THEORY: $n_r = 2 - Re_{r,p}$

EXPERIMENT: n_r FROM FIG. 24 (ASSUMES $Re_{r,t} = Re_{r,p}$)

2144-PORT INJECTION

SYMBOL	$Re_{t,j}$
○	120,000
△	240,000
□	360,000

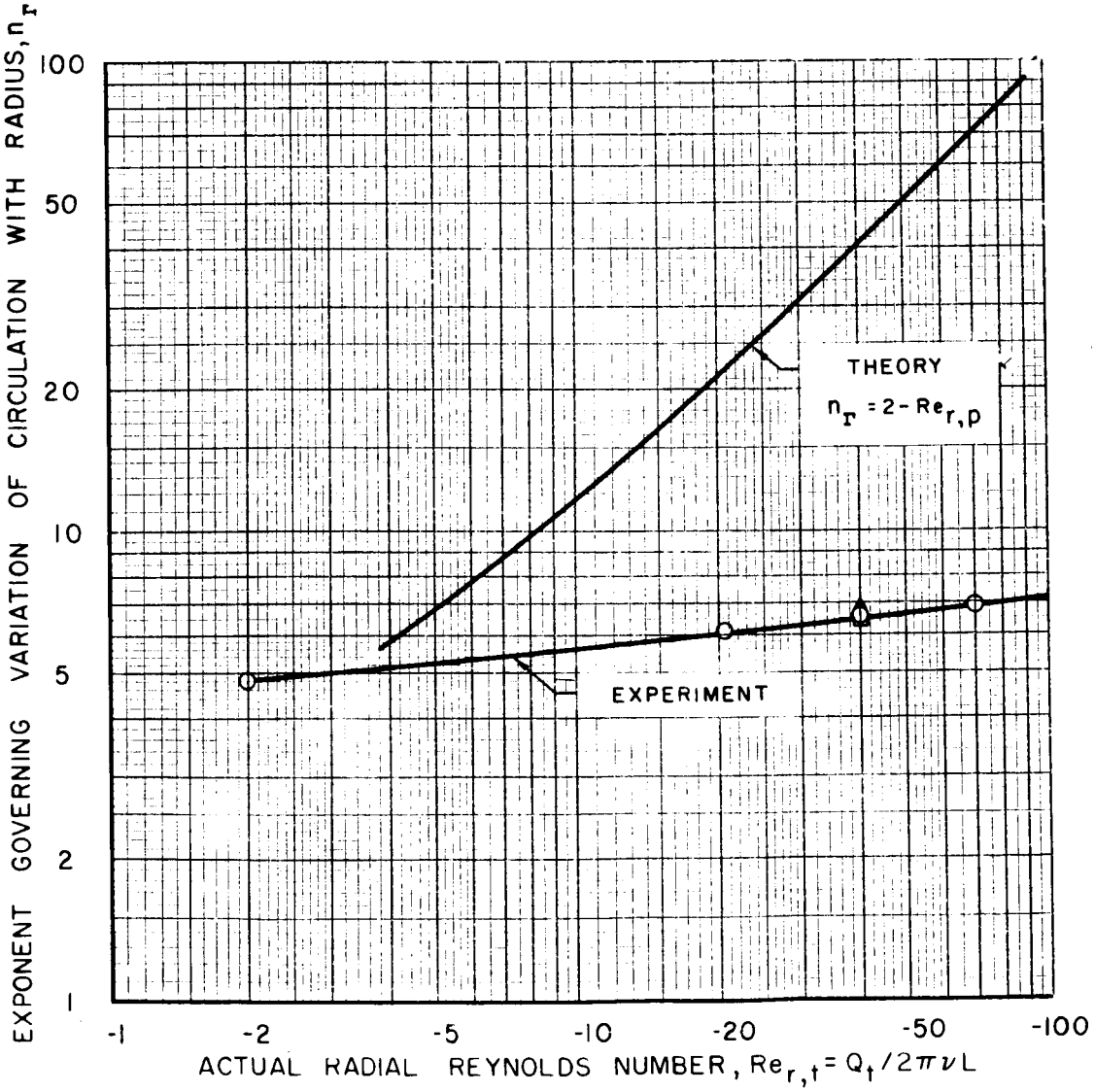

FIG. 26

EFFECT OF OUTFLOW RADIAL REYNOLDS NUMBER ON RATIO OF EDDY VISCOSITY TO LAMINAR VISCOSITY WITH FLUID INJECTION THROUGH CENTERLINE POROUS TUBE

$Re_{t,j}$ = 120,000

2144-PORT INJECTION

$$\frac{\rho\epsilon+\mu}{\mu} = \frac{(2-n_T) \text{ FROM LAMINAR THEORY (SEE FIG. 25)}}{(2-n_T) \text{ FROM EXPERIMENT (SEE FIGS. 24 AND 25)}}$$

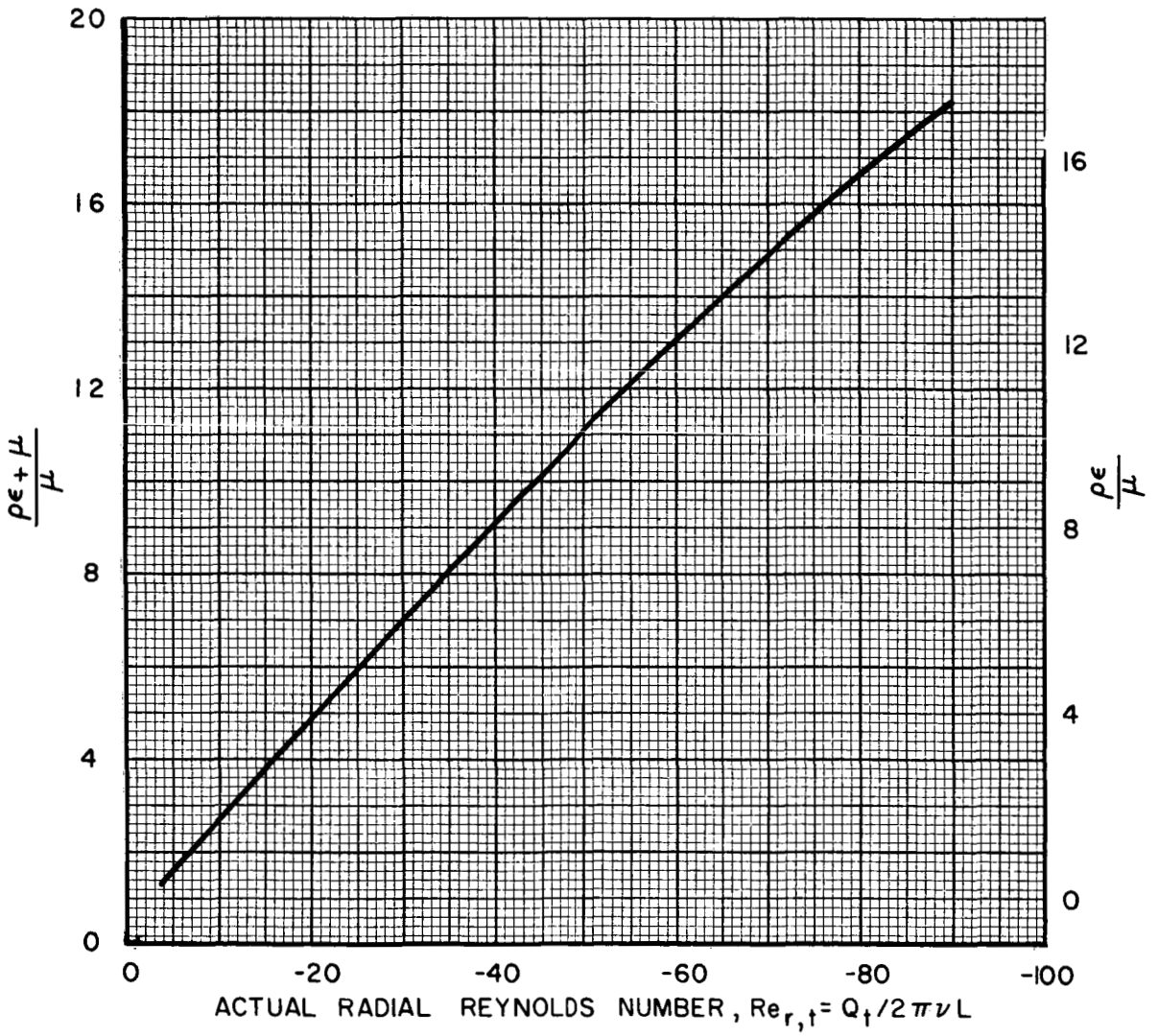

MICROFLASH PHOTOGRAPHS OF DYE PATTERNS WITH FLUID INJECTION THROUGH CENTERLINE POROUS TUBE

RADIAL REYNOLDS NUMBERS OF -3, -30, -60, AND -100

$Re_{t,j} = 120,000$

2144 - PORT INJECTION

SEE FIG. 2 FOR DETAILS OF INJECTION CONFIGURATION

DYE INJECTION THROUGH CENTERLINE POROUS TUBE

FLOW ROTATION